1. Author's responses to Reviewer comments

We gratefully thank the three Reviewers for their suggestions and comments. Below we present our response to each Reviewer. General comments are considered first, which are followed by point-to-point answers to specific comments. (The Reviewer comment is shown in *italics* and highlighted with yellow, which is followed by our response in plain text).

The relevant changes in the manuscript are highglighted in orange.

1.1 Reviewer #1

General comments

This paper describes an analysis of surface-based remote sensing observations of a stratus boundary layer over few days. The observations are taken at a coastal site (Mace Head, Ire). The analysis features vertical motions from a Doppler lidar plus some ancillary data from a cloud radar (principally used to define cloud top). Conditions vary diurnally and synoptically over the observation period. The authors concentrate on profiles of properties of the vertical velocity variance sprectrum including the variance, skewness, spectral peak, and rate of dissipation of turbulent kinetic energy (TKE). The time series of these variables are interpreted in terms of a coupled vs de-coupled boundary layer.

In general the paper is reasonably well-written. The background and methodology sections are fairly straightforward and comprehensible. These sections are mercifully brief but provide enough information to make the paper self-contained. The discussion of meteorological conditions is lengthy and is almost a blow-by-blow description of the events of the entire period. To some extent this is needed to set the synoptic context of the changes that are observed. These are confusion factors in attempting to relate turbulence dynamical effects to local BL structure, etc. I confess I found this a bit hard-going, mostly because of the poor quality of Fig. 3-5, which are real eye-strainers. In section 4 the authors strive manfully to relate the estimated turbulent variables to important changes in BL structure and forcing. Decoupling is a key aspect. It is apparent that this is a messy business and just two days of data are not going to bring any clean insights.

In my opinion the paper represents a usable description of an amusing data set. The major weakness is that the authors provide little guidance on how their data are unique and if they have found new insights. Assuming they can do a little more homework on this, I recommend publication with minor revisions. I also have a few editorial comments for the author to consider.

We will adjust Figures 3-5 as noted by the Reviewer. For example, we will divide Figure 5 to two parts to be more easily viewed: the vertical velocity statistics will be given in a separate figure, and the averaging time will be extended from 30 min to 1 hour to produce a cleaner and more consistent presentation.

We will emphasize the motivation of this paper more clearly in the introduction, i.e. the paper demonstrates the versatility of continuous Doppler lidar measurements to characterize the boundary layer structure and focuses on providing additional information to support the diagnosis of the mixed layer properties based on vertical velocity statistics from the lidar. One of the goals is also to investigate how the transition between coupled and decoupled mixed layer states affect the inertial

subrange scaling at different height inside the boundary layer.

The motivation of the paper is further elaborated on from line 25 on page 3 to line 21 on page 4.

Specific comments

1.
I suggest the authors make it painfully clear that their turbulence observations are essentially sub-cloud only. See Ghate et al. (JAMC, vol 53, p117-135) for an example of combined lidar and radar turbulence observations.

We will note this in the Introduction, it says “Unless otherwise mentioned, our analysis focuses on the properties of the below-cloud portion of the boundary layer only, in contrast to e.g. Ghate et al. (2014), who employed a combination of data from a Doppler lidar and a cloud radar”.

This is mentioned in lines 3-6 on page 4.

2.
*The parameter Lambda0 is actually the wavelength associated with the wavenumber peak of k*S(k). I don’t know why you would refer to it as a ‘cut-off wavelength’.*

The 'cut-off' refers to the maximum wavelengths that belong to the inertial subrange. We will adjust the wording to “transition wavelength” throughout the manuscript.

3.
Suggest given a value for a (eq. 4). Did you state what value you used for mu?

For *mu* we tried a few different values. *mu* = 1 gives the von Karman spectrum, but we ended up with a value of 1.5 as it better matched most of the observed spectra and provides a sharper curvature of the spectrum at the transition between -5/3 slope and the smaller wavenumbers. For this, *a* is approximately 0.69.

This is stated in Section 2.2, lines 18-19 on page 7.

4.
*As an alternative to eq. 6, you can use the value of kˆ(5/3)*S(k) for wavelengths smaller than Lanbda0 to compute epsilon. It would be interested to see how those values compared.*

We tested this by calculating the dissipation rate from the vertical velocity spectra for the period 12-18 UTC on the 24th of Feb in Mace Head at the three heights used for spectral analysis in the original manuscript. We used the fitted spectral model (Section 2) for the integration over the wavenumber space in order to get better representation at the short wavelengths. The results are shown in Figures 1 and 2 at the end of this document. For small dissipation rates the method suggested by the Reviewer compares pretty well with those from Eq (6) in the manuscript (based on O'Connor et al. 2010, Figure 1 below). For larger dissipation rates, the method suggested here tends to underestimate as compared to the values from Eq (6). Figure 2 of this document shows that at low altitudes the agreement between the two dissipation rate samples is relatively ok, while at higher altitudes there is somewhat more variation in the dissipation rates from Eq (6) than in the

ones from the method suggested by the Reviewer. The main reason why the method based on Eq6 gives more scatter in the dissipation rates is that they were derived using just a 2-minute window for processing the raw Doppler retrievals, while our spectral analysis uses samples over 30 minutes. Of course, other possible contributing factors range from accuracy of our spectral retrievals to possible shortcomings in the original dataset. A more in-depth investigation into this might be a topic for another study.

This comparison is reported only in this document since they do not impact the analysis or the results in the manuscript.

5.
One well-used index of decoupling is the difference in the lifting condensation level (LCL) and the observed cloud base height. Is it possible to provide that?

Unfortunately, no collocated thermodynamic profile measurements were available with the lidar measurements. However, we have attempted using the operational soundings from Valentia, although it is pretty far away from Mace Head. Nevertheless, the surface based LCL in Valentia is generally much lower than the actual cloud base height in Mace Head on Feb 24th (300-500 m LCL vs. ~900 m cloud base, thus LCL is pretty well in line with the zero-skewness height). Towards the night and on Feb 25th the LCL increases to about 600-650 m which is relatively close to the cloud base height in the morning hours. This stems from the fact that the cloud layer becomes more strongly coupled with the surface due to intensified cloud generated turbulence which encroaches into the weakly turbulent surface layer.

The radar dataset we used in this paper with CloudNet processing includes collocated model data profiles (the Met Office unified model UK4 in this case). Thermodynamic profiles and LCL were analysed from the model data as well. The data shows hints of a decoupled structure early in the afternoon but most of the time this is not visible. However, the lidar profiles of dissipation rate and vertical velocity variance do indicate a decoupled structure during the afternoon of the 24th and thus we suspect that the model has trouble adequately describing the decoupled structure. This is seen by e.g. by comparing the statistics profiles from the 24th and the 25th, the latter showing a quite characteristic cloud driven but well mixed more strongly coupled boundary layer.

We will briefly note the Valentia soundings. Moreover, we will provide additional line plots of the statistical profiles as suggested by Reviewer #3 to provide a more detailed presentation (Figs 6 and 7 in the revised manuscript).

Valentia soundings are commented on in lines 13-17 on page 12. In addition, LCL was analysed from surface temperature and humidity measurements. These are noted in line 10-12 on page 12 and in the Conclusions, lines 6-7, page 20. The LCL is also depicted in the revised Figure 5.

6.
Speaking for myself, I don't think Fig. 2 adds much to the paper and could be eliminated.

We will eliminate the figure from the manuscript.

The figure is eliminated.

7.
I found the cloud mask shown in Fig. 6 to be useful, suggest it be added to Figs. 4-5. Also suggest enlarging Fig. 5 to make it easier to see.

We will add the cloud mask to the plots of vertical velocity statistics. We will divide Figure 5 into two parts for it to be more easily viewed ("raw" data and statistics separately).

The old Figure 5 is now presented in Figures 4 and 5 of the revised MS.

1.2 Reviewer #2

General comments

The paper's background is succinct and straightforward, the methodology is sound, and the synoptics of the intensive observation period is adequately described. I question the validity of the interpretation of BL vertical structure based on turbulence-scale Doppler lidar kinematic data, especially given the lack of thermodynamic data. Below, I make some suggestions that may corroborate or contradict this interpretation. This probably requires more than a major revision, and certainly would fundamentally alter the paper.

While the basis for this conclusion is correct, the paper does not exclude other factors that may explain the change in w skewness. I see this as the main weakness in this paper. I am especially skeptical because the Doppler lidar wind speed profiles (Fig. 4) do not show any shear layer corresponding with the "decoupling height" (the height of the interface between surface-based and cloud-driven mixing), and because the lidar backscatter power (Fig. 5a) does not show an aerosol layer corresponding with the same stable layer.

The main remedy I suggest is to use proximity temperature and humidity profiles (e.g., from radiosondes) to show the decoupling, and the evolution of the decoupling height. It would be very nice to quantify decoupling strength at the interface. This would be the nail that seals the case, but presumably, such data are not available. In that case the paper will be much weaker, but some venues can be explored to seek further evidence. Six possible venues are listed below.

There is indeed a lack of thermodynamic data, which is addressed further in our responses to the specific comments by the Reviewer. We will add discussion about other possible contributing factors to the vertical velocity statistics in the manuscript. However, even though we cannot provide an estimate for the decoupling strength, we do argue that the kinematic data does make a point for the decoupled boundary layer structure, as further discussed in our responses below. However, we will revise these considerations as the turbulence in the surface layer is mostly very weak and we will also add discussion about the reasons behind it to Sections 4.1 and 4.2 as suggested by the Reviewer.

We have now included estimates of the LCL based on surface measurements in the manuscript, which also support the interpretation of a decoupled boundary layer (shown in the revised Figure 5). The rest of the changes in the manuscript are outlined below in the specific comments.

1.
Explore the flow field relative to the terrain near Mace Head, which appears to be close to a cliff overlooking the ocean. As the wind speed decreases around t=18 hrs in Fig. 4, there may be a shallow layer of offshore or drainage flow. Fig. 4 could be reproduced for wind direction. Changes in wind direction can produce changes flow relative to the terrain and changes in stability, and thus in vertical velocity moments.

We will add the suggested figure. As the wind speed and vertical velocity turbulence are quite weak after 18 UTC, especially near the surface, it is possible that the vertical velocity skewness values are

not physically significant at this time.

We will consider these comments in Section 4.1.
This is discussed in line 13, page 25 – line 3, page 26 and line 20-24 on page 14.

2.
It is not clear how the decoupling height diagnosed from the profiles of w skewness. The w skewness field based on 30 min intervals is quite noisy (Fig. 5d). It often changes sign over the full depth of the BL from one instance to the next. The velocity uncertainty increases with decreasing SNR or power, which is quite obvious from a comparison between Fig. 5a and d. It would be good to see whether the pattern becomes more crisp (or vanishes) under different velocity QC, processing, and averaging periods.

We attempt to approximate the decoupling height as the level where the vertical velocity skewness changes sign. We have experimented with longer averaging times and the negative skewness structure indeed becomes somewhat more robust with longer averaging. The skewness profiles remain quite consistent with the dissipation rate and variance profiles.

We will revise the figures showing vertical velocity statistics and analysis of the height of the layer interface using 1-hour averaging timesteps instead of the 30 mins in the original manuscript to provide a cleaner presentation. We will also add new figures (6 and 7 in the revised manuscript), which present line plot profiles of the vertical velocity statistics in more detail, with 1-hour averaging time. The velocity estimates used for calculating the statistics are subject to SNR threshold based quality control as well as to methods presented in O'Connor et al. 2004. In addition, the methods presented in O'Connor et al. 2010 were used to correct the dissipation rate for observation based errors.

We will elaborate on the methodology in Section 2.2. In addition, in Section 4.2, it will be more explicitly shown that scaling of L0 supports the skewness-based decoupling height estimate, at least for periods with pronounced separation in the skewness-profiles.

The methodology is revised in lines 2-7 on page 8. The comment is also considered in the results, in lin 19, page 16 – line 2, page 17. The vertical velocity statistics show in the revised Figure 5 are now obtained using 1-hour averaging time.

3.
Repeatability is always useful. This is a case study of a 24-36 hr period. Do the same relations apply in other fair-weather Sc-topped BL conditions?

The synoptic situation is quite common in mid-latitude winter marine environments and the boundary layer properties are not influenced by anything extraordinary. Unfortunately, given the instrumentation at our disposal, it has been difficult to find measurements which could be used for a similar spectral analysis. This is essentially because of two things: First, the analysed period from Mace Head provided quite a unique set of data in terms of quality and prerequisites for spectral analysis. The marine air mass provided sufficiently strong signal with our lidar instrumentation, so that the vertical velocity data wasn't too noisy for deriving the power spectra. Related to this, the SNR of the velocity retrievals can be improved by increasing the integration period for individual velocity samples, yet as a downside, too long integration periods make it impossible to derive meaningful spectra, since (with Taylor's hypothesis in mind) it will mask out higher wavenumbers. Second, the wind speed during the analysed period was moderate (below 10 m/s) which also contributes to better sampling of the higher wavenumbers. Similar instruments to those used in the manuscript have been employed in different parts of Finland by the FMI. Generally, in continental

sites, the instruments are not able to provide strong enough signal below the cloud base for robust vertical velocity retrievals at sufficient time resolution, at least for spectral analysis. However, statistical profiles can be derived more often and similar structures of skewness and variance profiles can be identified in marine environments, such as that in the Utö island in the Finnish archipelago. In a future study it is thus possible to extend this investigation and quantitatively study the occurrence of the boundary layer structure reported in this paper with data from different sites. However, for the present manuscript, we stick to the Mace Head data.

4.
Much can be learned from the variation of w power spectral density with height across the interface. If the paper's main conclusion is correct, then one can expect a minimum in TKE near the decoupling height, simply because of distance from the TKE generation regions, i.e. the cloud top layer and the surface. This is unlikely to be the case, because TKE and turbulence dissipation rate tend to strongly correlate, and the computed turbulence dissipation rate (Fig. 5e) does not appear to have a minimum near the decoupling height (Fig. 6), although the time axes do not match so it is difficult to compare the two Figs.

Line plot figures presenting profiles of vertical velocity variance, skewness and the dissipation rate will be added to the manuscript. They show in detail that on many occasions on the 24th Feb the dissipation rate (and thus presumably TKE) is clearly strongest in the upper part of the boundary layer near the cloud deck. Similar results are seen for the standard deviation as well. Especially in the afternoon there is often a sharp decrease in the dissipation rate below the height of decoupling, and the turbulence near the surface actually remains quite weak. Thus we expect it would be difficult to resolve a clear minimum in the turbulence intensity near the decoupling height (though that kind of structure can actually be seen at least on one occasion where mixing close to the surface is intensified for a short period). We will add discussion about this point in Section 4.1.

Moreover, the boundary layer on the 25th of Feb, after midnight, appears essentially well mixed, but the statistical profiles provide strong indication that this is cloud driven as well. There is also a clear contrast in the structure of the profiles as compared to the afternoon of the 24th. This will be elaborated on in Section 4.1 as well.

The shapes of the dissipation rate profiles are now discussed in lines 7-12 on page 14 according to the response above.

5.
Cloud-top driven mixing (or cloud top entrainment instability) has been shown to be active in various Sc environments (see review by Woods 2012). It is only hypothesized to be active in this case. Profiling Doppler radar data within the drizzle layer should reveal the presence of vertical velocity turbulence. I believe these data are available.

Profiles of the vertical velocity variance and skewness in the drizzle layer are shown in Figures 3 and 4 of this document. There is considerable mixing observed in the drizzle layer as sigma_w is about 0.4 m/s through much of the depth of the layer on 24 Feb and even stronger on 25 Feb. Moreover, especially on 24 Feb, the skewness is predominantly negative or around zero within the cloud layer, which is expected. Further, on 25 Feb, positive skewness values are seen at approximately the base of the cloud, while below-cloud profiles from lidar (Fig 7 in the revised manuscript) show increasingly negative skewness towards the surface, which is expected for cloud-driven well-mixed boundary layer.

We will comment on these results in Section 4.1 but prefer not to include more additional figures. It now says “The collocated Doppler cloud radar observations also indicate considerable turbulent activity within the cloud layer”.

This sentence is added in lines 19-20 on page 11.

6.
Decoupling strength can be estimated from the difference in potential temperature at the surface and that at cloud base. The latter may be available from a zenith infrared thermometer. If not, then the difference between the lidar-determined cloud base height and surface-based LCL is a good measure of decoupling strength, although it will not give the decoupling height.

As stated, we do lack the thermodynamic profiles. Compared to the LCL from operational soundings at Valentia the cloud base height observed at Mace Head is much higher (300-500 m LCL vs. ~900m cloud base). The model data profiles provided with the radar datasets generally seem to miss the decoupled structure (please refer to comment 5 by Reviewer #1). We argue however that the kinematic statistics do show a clear indication of the decoupling, since in many cases the variance, as well as dissipation rate peak near or within the cloud layer and decrease towards the surface. In addition, the scaling of L0 generally supports these results.

We will briefly comment on the Valentia soundings in Section 4.1. Although they are pretty remote from the lidar observation site and thus can not be regarded as very strong evidence, the meteorological conditions are somewhat similar to those in Mace Head at least towards the afternoon.

We did include LCL derived from surface measurements to the manuscript. It is given in the revised Figure 5 and commented on in lines 10-13 on page 12.

Minor comments

1.
The theory in Eqns 1-6 is sound but the text does not specify the value chosen for the variable mu.

We ended up using the value 1.5, which generally provided the best fit to the observed spectra, and causes the curvature over the transition from the -5/3 slope to outer scales to be slightly sharper than that in von Karman spectrum with mu = 1. We will elaborate on this in Section 2.2 (See also our response to the 3rd comment of Reviewer #1).

This is now given in lines 18-19 on page 7.

2.
Table 1: add units to range resolution (m)

This is corrected.

3.
Fig. 1: please use real data to make the point. The power spectral density curve shown is physically impossible.

This is replaced with an actual example.

4.
It is not quite correct to use "time (hours UTC)" in the abscissa title of most figures. One option is to use "time since 00 UTC on 24 Feb 2012 (hours)".

This is corrected.
5.
Fig. 6: The black region is NOT the cloud layer. Rather, it is the drizzle layer, which often extends below cloud base. A Ka-band radar can only detect drizzle-size drops (e.g., Fox and Illingworth 1997).

In Figure 6 the cloud base is determined from the lidar data, while radar is used to determine only the cloud top, which is generally invisible to the lidar (This was mentioned already in the original manuscript, p. 24132, lines 23-24). Therefore the black region can be expected to provide a rather good estimate of the vertical extent of the cloud layer.

Determination of the cloud mask is elaborated on in lines 4-9 on page 11.

6.
The evaluation of upper wavelength of the inertial subrange (lamda_o) in Figs. 6 and 7 is done at three heights within the BL, whose depth is based on the radar profiles (cloud echo top). These heights cut across the decoupling height. If indeed the surface-driven layer clearly is decoupled from the cloud-driven above, it would be more interesting to characterize lamda_o in this two respective layers.

We performed additional analysis where L0 is analysed at two levels, one inside the surface layer and one in the cloud driven mixed layer (in the middle of the layers). The results show that L0 sampled from the cloud driven layer scales pretty well with the corresponding layer depth, even though the variability is rather high. The surface-based L0 shows quite robust scaling during pronounced separation in the profiles of skewness between the surface and cloud-driven regimes, while for most other instances, similar results are not seen.

We will update the original Figures 6 and 7 accordingly and elaborate on these results in Section 4.2.

The scaling of the inertial subrange in these figures is now sampled more consistently and the depth of the corresponding mixed-layers is used as the normalizing factor. Discussion of these results in Section 4.2 is revised accordingly.

1.3 Reviewer #3

General comments

1.
The authors seem to have a conceptual model in mind, which should be made more explicit in the Introduction. This would make the paper more accessible to a wider audience, rather than just measurement specialists. Their model is first referred to in section 4, and seems to be based on the idea of "competition" between surface- and top-driven convection. In fact, both surface and top driving may be present, and cooperate (rather than competing) to produce turbulence. When thinking purely of skewness, the two drivers do have opposing effects. The questions that should be addressed by the analysis are: What are the depths of influence of surface and top

driving? When do the two depths merge to create a single turbulent layer, and when do they remain decoupled? What is the degree of coupling, since coupling is a continuum between fully coupled and fully decoupled? The last question can be addressed by emphasizing variance profiles. Another issue is what processes are reducing coupling (or increasing stability), since turbulence always acts to reduce stability?

We will revise the idea of competition, which indeed does refer to the opposing signs of skewness, that also is an indicator of the direction of the transport of turbulent kinetic energy. It is also a fact that during the 24th, the surface layer is mostly quite weakly turbulent, so that the influence of surface-based processes on the state of the entire boundary layer is likely relatively weak and the boundary layer structure depends more on the factors that influence the intensity of the cloud generated mixing. Moreover, the scaling of L0 from the different layers can perhaps be used to infer the depth of influence of the more intense cloud-driven layer.

We will elaborate on our point of view on the impacts of different layers of the boundary layer structure in the Introduction. We will also include additional discussion about the points raised by the Reviewer in Sections 4.1 and 4.2.

The point of view for this analysis is further explained in lines 12-21 on page 4, and the analysis of the results has been elaborated on in Sections 4.1 and 4.2.

2.
In addition to the figures already included, some line plots of vertical profiles of variance and skewness during the different regimes (appropriately time-averaged) should be shown. This will allow the reader to understand better the data presented in the time-height plots.

We will add line plots with vertical velocity statistics averaged over 1 hour segments for the afternoon of the 24th and the morning hours of the 25th which nicely present the key differences between the two cases (Figs 6 and 7 in the revised manuscript).

These will be commented on in Section 4.1.

New figures 6 and 7 have been added and discussed in lines 3-9, page 12 and lines 21-23, page 12.

3.
Throughout the paper, the vertical coordinate is scaled by the cloud-top height, which is defined as the boundary layer height. This is not treated completely consistently, since it is acknowledged later that the expectation is that each sublayer should scale with its own depth.

We will adjust the normalizing issue in the manuscript and change the normalization to account for the sublayer depths. Our results show that L0 sampled from the cloud driven layer scales rather well with its own layer depth. Similarly, during periods when the surface layer deepens (as during 12-15 UTC on the 24th), L0 sampled near the surface also scales well with the corresponding depth. However, the same is not always true for weaker separation between the cloud-driven and surface-based layers as diagnosed from the skewness profiles.

We will revise the methodology in Section 2.2 and the adjust the analysis accordingly in Section 4.2.

The figures 8 and 9 in the revised manuscript now show the scaling of the inertial subrange

analysed for the cloud-driven and surface-based layers, with the corresponding layer depth used as the normalizing factor. Presentation of the results in Section 4.2 has been updated accordingly.

Specific comments

1.
In the last paragraph of section 4.1, the attribution of the measured effects on the boundary layer is unclear. Is there really an influence of the land, even though the flow is still onshore? Advection of cooler air aloft would also reduce stability and increase mixing, can this be ruled in or out?

We cannot strictly rule this out and we will consider this possibility in Section 4.1. It says:

"Further, Fig. 3 suggests some height-dependent fluctuation of the horizontal wind during this period. The fluctuations might act to trigger periods where the stability near the surface is reduced, allowing a surface-based TKE production to affect a deeper layer. In particular, we cannot rule out the possibility of advection of cooler air aloft, which could potentially act as a driver for such events. At the same time, this could also act to slightly increase the stability in the upper portion of the boundary layer, further contributing to the relative strengths and extent of the cloud-driven and surface based mixed layers."

This discussion is found in line 26, page 13 – line 3, page 14.

2.
In section 4.2, it is indicated that the spectra have various structures. It might be helpful to include some representative spectra in a supplement.

As suggested by Reviewer #2 we will replace Figure 2 with an example from actual data which show the typical retrieval from which L0 is inferred. The different "structures" that sometimes take place are mainly just artifacts due to noisy retrievals.

An example of the retrieved spectra is given in Fig. 1.

3.
page 24133, paragraph beginning with line 19: Does L0 scale with the horizontal size of the clouds or breaks, rather than the layer depth?

No robust dependence is found. This kind of behavior might be found for surface-based cumulus convection. Here L0 appears to be mainly controlled by the TKE generation at cloud top and the resulting BL structure: This paragraph is adjusted according to the revised analysis of the inertial subrange scaling (following the general comment no.3 by the Reviewer).

The discussion in line 13, page 16 – line 11, page 17 is revised accordingly.

4.
page 24133, line 27: Here is a particular example of the conceptual model issue. In what sense do the surface and top driving compete to prevent formation of a mixed layer? Don't they in fact cooperate, but with possibly differing strengths?

We were focusing on the predominate direction of the flux of kinetic energy that can be inferred by

investigating the sign of the skewness parameter, thus indicating the dominant source of energy in each layer which we attempt to use to characterize the boundary layer structure.

In accordance with the Reviewers notion, we will revise this terminology throughout the manuscript and elaborate the idea in the Introduction.
The suggested revision has been implemented throughout the manuscript.

5.
page 24134, line 11: Is the supression of L0 during this time real, or an artifact due to very weak turbulence?

For the surface-based samples, the weakness of turbulence might affect L0 during this time. However, this is not the case for the samples from the cloud driven layer, which also show relatively small L0 even a few hours after the cloud driven mixed layer covers essentially the entire boundary layer.

This discussion will be revised according to the new figure presenting L0 in Section 4.2. It says: "The suppression of the surface-based L 0 can also be due to artifacts introduced by the weakness the turbulent mixing".

This notion was eliminated while revising the manuscript but related modifications are found on line 25, page 17– line 5, page 18.

6.
page 24134, line 17: Wind shear at the cloud top influences entrainment, not wind in general.

This will be corrected.

This is corrected.

7.
page 24136, line 13: It should be expected that decoupling reduces L0 as it is defined here, since in a decoupled structure scales should go with their own layer depth, not the depth of the whole structure. This is consistent with the statement of previous expectation in lines 25-26.

We will revise this statement. It will be acknowledged that L0 from the cloud driven regime does scale relatively well with the mixed layer depth. However, it is noted that this is not always true for L0 in the surface layer, except when the surface layer extends to more considerable depths into the boundary layer.

The revised discussion is found on line 13, page 20 – line 2, page 21.

8.
Figure 6 and text discussing it: It should be acknowledged that surface-driven layers without cloud have negative skewness near their tops.

It now says is Section 4.1:
"... negative skewness of vertical velocity, which has been shown to indicate cloud-driven mixing (Hogan et al., 2009), is a predominant feature of the below-cloud mixed layer (although it can also

be observed near the tops of clear-sky surface-driven layers)".

This is acknowledged on line 26, page 11.

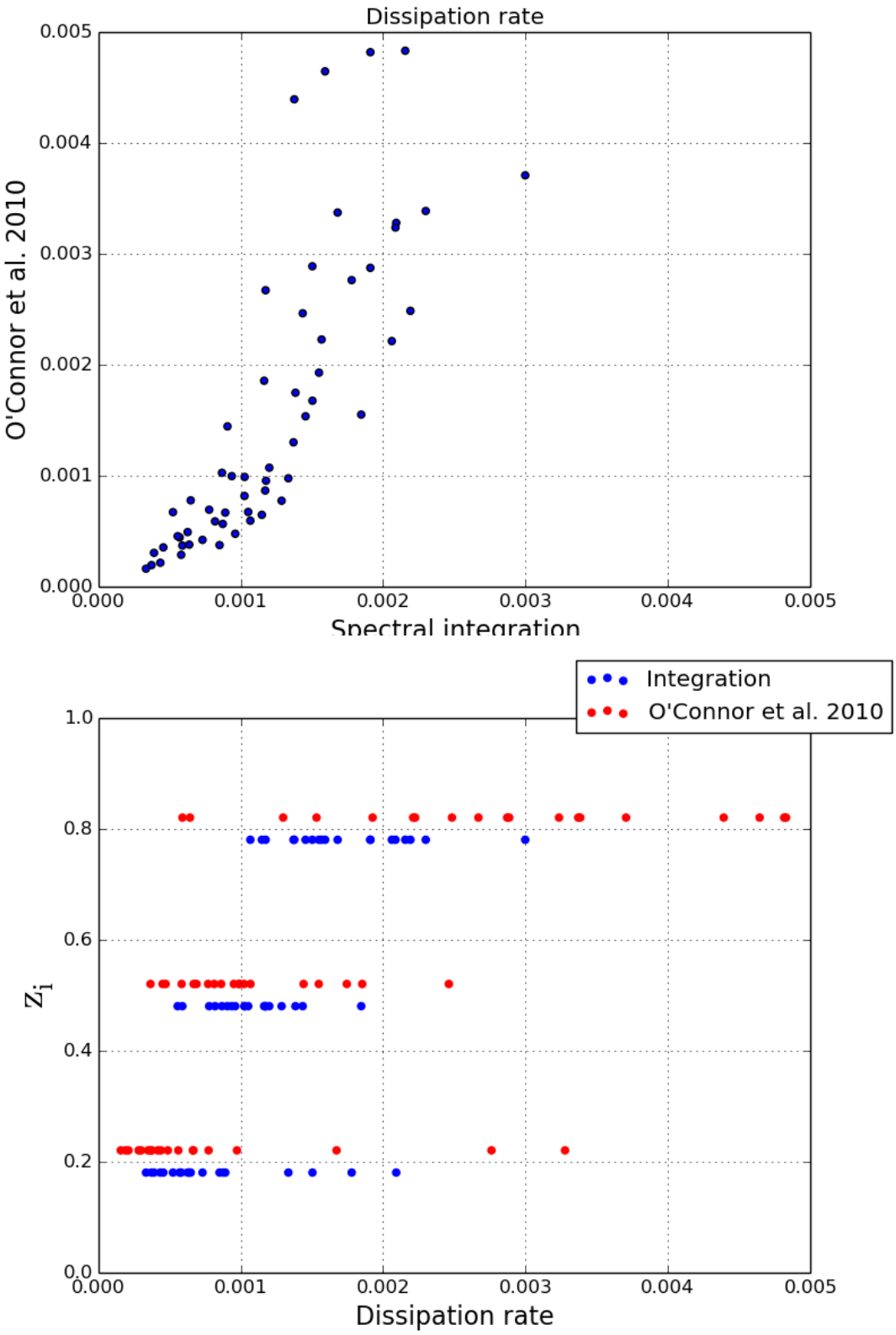

Figure 2: Same as Fig. 1 but analysed separately at three sampling levels (normalized by the boundary layer depth diagnosed from cloud top height). The samples are from the same altitudes but a small offset is applied in the figure for better presentation.

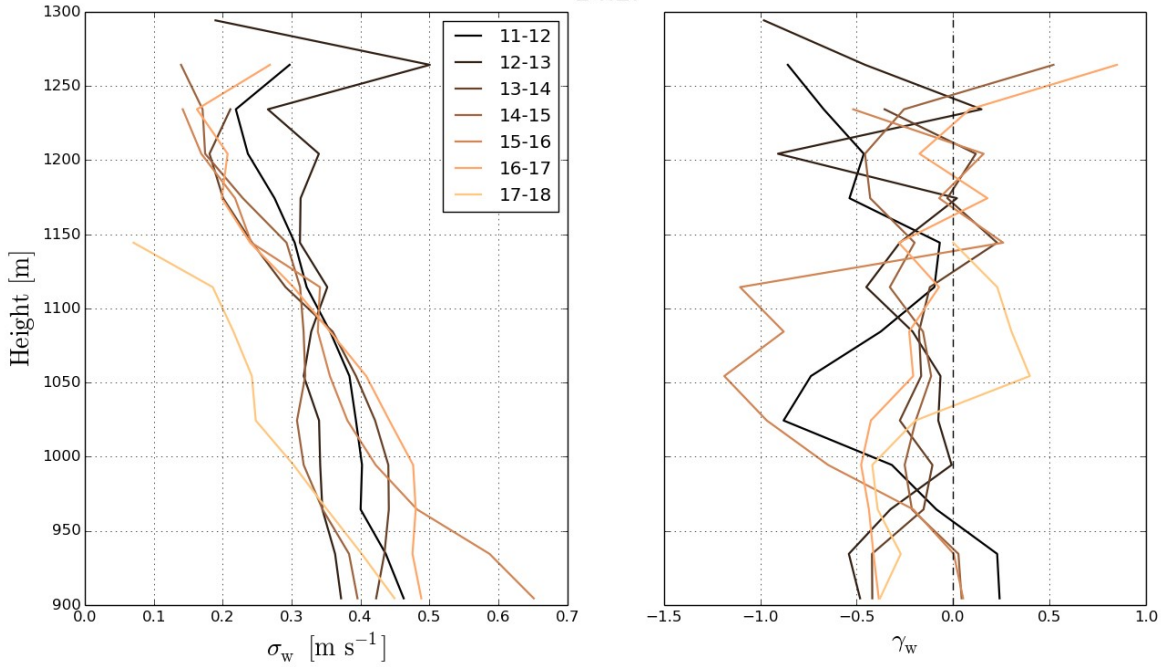

Figure 3: In-cloud standard deviation and skewness of vertical velocity as derived from a Doppler radar on 24 Feb (the height range presented corresponds roughly to the thickness of the cloud).

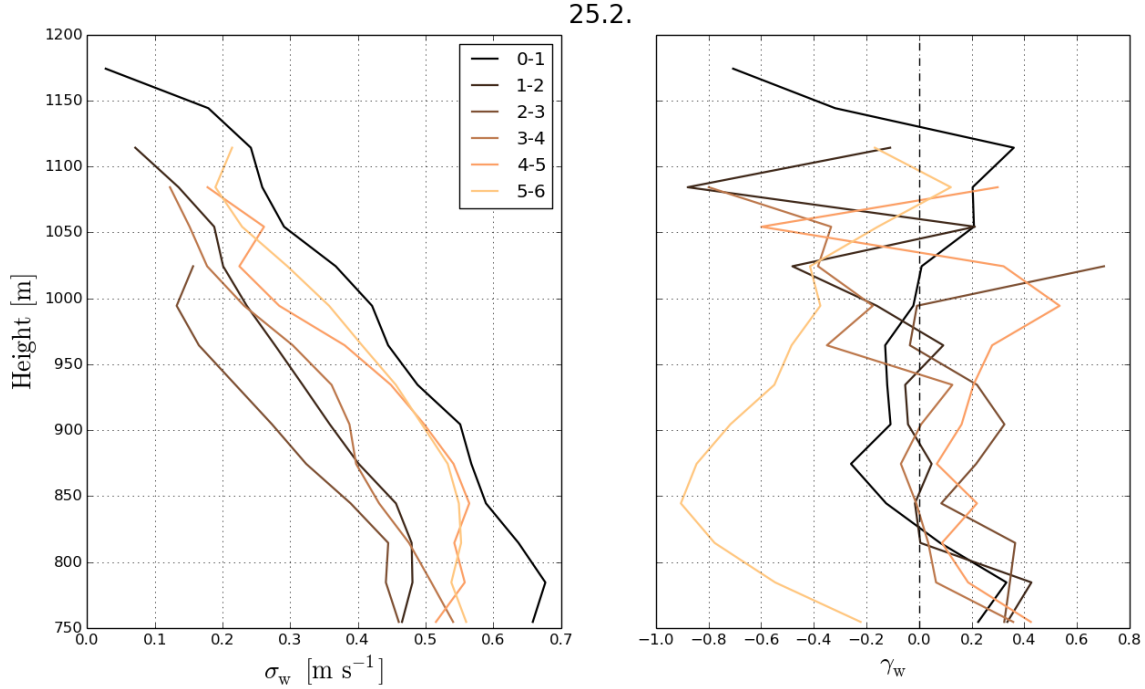

Figure 4: In-cloud standard deviation and skewness of vertical velocity as derived from a Doppler radar on 25 Feb (the height range presented corresponds roughly to the thickness of the cloud).

[1,3]J.Tonttila [2,4]E. J.O'Connor [2]A.Hellsten [2,5]A.Hirsikko [6]C.O'Dowd [3]H.Järvinen [2]P.Räisänen
Manuscript prepared for Atmos. Chem. Phys. Discuss.
with version 2.2 of the LaTeX class copernicus_discussions.cls.
Date: 24 April 2015

Turbulent structure and scaling of the inertial subrange in a stratocumulus-topped boundary layer observed by a Doppler lidar

Finnish Meteorological Institute, Atmospheric Research Centre of Eastern Finland, P.O. Box 1627, 70211 Kuopio, Finland

Finnish Meteorological Institute, P.O. Box 503, 00101, Helsinki, Finland

University of Helsinki, Department of Physics, P.O. Box 48, 00014, Helsinki, Finland

University of Reading, Reading, UK

Forschungszentrum Jülich GmbH, Institut für Energie-und Klimaforschung: Troposphäre (IEK-8), Jülich, Germany

School of Physics and Centre for Climate & Air Pollution Studies, Ryan Institute, National University of Ireland Galway, University Road, Galway, Ireland

Correspondence to: J. Tonttila (juha.tonttila@fmi.fi)

Abstract

The turbulent structure of a stratocumulus-topped marine boundary layer over a two-day period is observed with a Doppler lidar at Mace Head in Ireland. Using profiles of vertical velocity statistics, the bulk of the mixing is identified as cloud-driven. This is supported by the pertinent feature of negative vertical velocity skewness in the sub-cloud layer which extends, on occasion, almost to the surface. Both coupled and decoupled turbulence characteristics are observed. The length and time scales related to the ~~cloud driven~~ cloud-driven mixing are investigated, which are shown to provide additional information about the structure and the source of the mixing inside the boundary layer. They are also shown to place constraints on the length of the sampling periods used to derive products, such as the turbulent dissipation rate, from lidar measurements. For this, the ~~upper cut-off wavelength of~~ maximum wavelengths that belong to the inertial subrange ~~is~~ are studied through spectral analysis of the vertical velocity. ~~The bulk statistical profiles and the scaling~~ The maximum wavelength of the inertial subrange ~~show consistent behaviour as the boundary layer undergoes transitions between a coupled and decoupled stratocumulus layer . The cut-off wavelength~~ in the cloud-driven layer scales relatively well with the corresponding layer depth during pronounced decoupled structure identified from the vertical velocity skewness. However, in many occasions, combining the analysis of the inertial subrange ~~does not appear to scale robustly with the relative depth of the local mixing regime at different altitudes during decoupled periods. Rather, the competition between surface-based and cloud-driven mixed layers suppresses the range of eddy sizes at all heights inside the boundary layer.~~ and vertical velocity statistics suggests higher decoupling height than expected from the skewness profiles. Our results show that investigation of the length scales related to the inertial subrange significantly complements the analysis of the vertical velocity statistics, and enables a more confident interpretation of complex boundary layer structures using measurements from a Doppler lidar.

1 Introduction

Properties of the turbulent variations in vertical velocity, as well as the scaling related to that variability, are important aspects for understanding boundary layer evolution, transport of momentum and thermodynamical properties. These aspects are tightly coupled to the formation and evolution of boundary layer clouds, which in turn strongly affect the radiation budget of the Earth's surface and thus the climate.

Measurements of the turbulent fluctuations of vertical wind in cloud-topped and clear-sky boundary layers as well as inside boundary layer clouds have been performed for decades, typically making use of in-situ measurement devices mounted on research aircraft (e.g. Duynkerke et al., 1995; Nicholls, 1984, 1989). Unlike in-situ sensors, active remote-sensing instrumentation based at the surface has the significant advantage of being able to routinely measure the velocity profile simultaneously at many levels. A variety of instruments have been employed for this task, from UHF wind-profilers (e.g. Gossard et al., 1998; Jacoby-Koaly et al., 2002) to SODARs (e.g. Kouznetsov et al., 2007), Doppler cloud radars (e.g. Shupe et al., 2012), and combinations of these (e.g. Norton, 2006).

Doppler lidars have the necessary high spatial and temporal resolution to derive turbulent properties (Gal-chen et al., 1992; Banakh et al., 1999); recent developments in this field have resulted in robust low-powered instruments designed to operate continuously and autonomously. They are ideal for boundary layer applications, where they have sufficient sensitivity. Since stratocumulus-topped boundary layers cover a significant portion of the globe, there have been numerous remote-sensing investigations of them in both marine and continental environments (e.g. Babb and Verlinde, 1999; Duynkerke et al., 1995; Frisch et al., 1995; Hogan et al., 2009; Kollias and Albrecht, 2000; Lothon et al., 2006; Moyer and Young, 1991).

In this article we investigate the scaling of turbulent eddies in a stratocumulus-topped boundary layer and its transition between different mixed layer structures. The analysed observations cover a boundary layer exhibiting marine characteristics, with both solid and broken cloud structure in the overlying stratocumulus deck. Doppler lidar measurements are used to analyse the vertical velocity field in the boundary layer below the cloud. The aerosol particles in the

marine environment provide an ideal tracer for the Doppler lidar and are present in sufficient quantities to provide measurements at high spatial and temporal resolution with good sensitivity throughout the entire vertical extent from near the surface up to cloud base. ~~This allows~~ Robust signal and high resolution allow for a Fourier analysis of vertical velocity as a function of height. The resulting power spectra are used to investigate the relative scaling of the turbulent eddies and contrast them with the bulk statistical properties of the vertical velocity distribution. ~~We can then attempt to link the turbulent variability with the nature of the boundary~~ The high-resolution, vertically resolved spectral analysis along with complementing profile data of the turbulence statistics is only possible using vertically-pointed Doppler lidars. This provides a unique and self-consistent dataset to study the relationships between vertical velocity statistics, the scaling of the turbulent eddies, as well as the source of kinetic energy in the mixed layer and the ~~overlying cloud deck.~~ general vertical structure of the boundary layer. Unless otherwise mentioned, our analysis focuses on the properties of the below-cloud portion of the boundary layer only, in contrast to e.g. Ghate et al. (2014) , who employed a combination of data from a Doppler lidar and a cloud radar.

Inspired through recent studies by Hogan et al. (2009) and Harvey et al. (2013), who provided observational evidence of how to identify and isolate the cloud driven mixing from surface-based mixing in a stratocumulus topped boundary layer based on the sign of the skewness of vertical velocity, we hypothesize that the scaling of the inertial subrange determined from the spectral analysis can be used as an additional diagnostic to identify the sources of turbulent mixing. ~~We also investigate how changes in the structure of the cloud deck affect this scaling in the sub-cloud layer in the situation where the turbulence is cloud-driven~~As the sign of the skewness indicates the direction of the flux of turbulent kinetic energy (TKE), the cloud driven and surface based layers can be seen to exhibit opposite and thus competing effects, depending on the relative strength of the sources of TKE and the stability of the mixed layer. It is then also expected that the scaling of the inertial subrange changes according to the mixed layer structure. This forms the basis for comparing the kinetic statistics with the scaling of the turbulent eddies, which we attempt to use in synergy to complement the individual diagnostics and thus to provide confirmation for the conclusions drawn about the boundary layer structure,

solely based on retrievals from the Doppler lidar instrument. We will also briefly discuss how the scaling of the inertial subrange and its evolution with changing boundary layer structure may affect scale-dependent lidar-based retrievals.

The layout of this paper is as follows: Sect. 2 describes the instrumentation and the main analysis methods. A description of the synoptic situation and key features during the analysed period is given in Sect. 3. The results obtained for turbulence statistics and the scaling of the inertial subrange are given in Sect. 4, followed by concluding remarks.

2 Methodology

2.1 Instrument

The data for this study were obtained from a coherent heterodyne pulsed Doppler lidar (production no 34) owned by the Finnish Meteorological Institute, and deployed at Mace Head, on the west coast of Ireland (53°19′ N, 9°53′ W), from 16 February to 27 March 2012 (Hirsikko et al., 2014). Operating specifications for the Doppler lidar are given in Table 1. Initial data points are oversampled at 3 m resolution and 10 points are then combined to give a final spatial resolution of 30 m. A total of 320 gates gives a maximum range of 9.6 km. The temporal resolution can be as high as 1 s. However, to obtain good sensitivity, it is usually necessary to integrate further, since useful signals are only obtained in the presence of a reasonable aerosol load, or when clouds are present.

The instrument was operated predominantly in the zenith-pointing stare mode, interspersed with a wind scan sequence every 10 min (giving 6 wind profiles per hour). For this campaign, an integration time of 10 s was selected for the vertical stare mode, sufficiently long for acquiring profiles with reasonably small uncertainties, while short enough for deriving turbulent properties.

As standard, the Doppler lidar provides profiles of signal-to-noise ratio (SNR), uncalibrated attenuated backscatter coefficient and radial Doppler velocity. Post-processing (Hirsikko et al., 2014) then applies background and focus corrections to the signal and provides calibrated at-

tenuated backscatter coefficient profiles, together with uncertainties in the signal, attenuated backscatter and Doppler velocity derived using an approximation to the Cramer-Lao lower-bound method (Rye and Hardesty, 1993) given in O'Connor et al. (2010).

The horizontal wind profiles were obtained using a 3-beam Doppler Beam Swinging (DBS) technique. The wind scan sequence consisted of three consecutive rays, one pointing to the zenith, and two orthogonal rays at 20° from the zenith (one pointing ~~North~~north, one pointing ~~East~~east). Vertical profiles of horizontal winds can then be obtained through trigonometry from radial velocities under appropriate conditions (e.g. Koscielny et al., 1984). As noted in Table 1, to reduce uncertainties in the retrieved horizontal winds, the integration time for each ray in the wind scan sequence was twice the integration time for an individual ray in the zenith-pointing mode. A single vertical profile of horizontal winds therefore took about 60 s to obtain.

Data quality is provided directly by examining SNR (after applying any background correction). The threshold is determined based on the acceptable uncertainty for a given application. For vertically-pointing data, the selected threshold of -21 dB for SNR is equivalent to an uncertainty of about ~~$0.05\,\mathrm{m\,s^{-1}}$~~ $0.05\,\mathrm{m\,s^{-1}}$ for this particular Doppler lidar instrument in this configuration. The Doppler lidar attenuated backscatter coefficient can additionally be calibrated according to a procedure introduced by O'Connor et al. (2004). In this method, the ~~integration~~ integral of attenuated backscatter from a nearly non-drizzling cloud base through to infinity is set equal to $1/(2\eta S)$, where η is the multiple scattering factor and S is the lidar ratio. Both η (close to 1) and S (20 sr) are assumed constant and known for this instrument and lidar wavelength in stratocumulus clouds (Westbrook et al., 2010). Drizzling clouds are screened from the calibration procedure by a non-drizzling condition. There it is required that attenuated backscatter coefficient values at 250 m below the cloud base are 10 times smaller than the attenuated backscatter coefficient inside the liquid cloud (O'Connor et al., 2004). The uncertainty in the calibration method is 20 %.

2.2 Vertical velocity analysis

The Doppler lidar produces vertical velocity profiles at 10 s resolution. Turbulent properties were derived from statistical properties of the vertical velocity distribution over longer intervals.

The properties are computed at every range gate of the lidar giving a high-resolution vertical profile of each turbulent property.

The second and third moments of the velocity distribution, standard deviation σ_w and skewness γ_w, are calculated from sequential vertical velocity samples over a ~~30~~60 min interval;

$$\sigma_w = \sqrt{\frac{1}{n}\sum_{i=1}^{N}(w_i - \overline{w})^2}, \; and$$

$$\gamma_w = \frac{\frac{1}{n}\sum_{i=1}^{N}(w_i - \overline{w})^3}{\sigma_w^3},$$

$$\sigma_w = \sqrt{\frac{1}{n}\sum_{i=1}^{N}(w_i - \overline{w})^2}, \; \text{and} \tag{1}$$

$$\gamma_w = \frac{\frac{1}{n}\sum_{i=1}^{N}(w_i - \overline{w})^3}{\sigma_w^3}, \tag{2}$$

respectively, where $\overline{w}$ is the sample mean vertical velocity and w_i is the ith vertical velocity sample. Due to the interspersed sampling of the horizontal wind every 10 min, n for the ~~30~~60 min period is in practice about ~~150.~~ 320.

The vertical velocity power spectrum is used to identify the range of scales over which turbulent mixing predominates, commonly known as the inertial subrange. This is accomplished by finding the ~~cut-off~~ transition wavelength λ_0 at which the spectral density peaks and the slope deviates from the expected $-5/3$-powerlaw, as shown ~~schematically~~ by an example from the analysed data in Fig. 1. The spectral model by Kristensen et al. (1989), also applied by Lothon et al. (2009), is used to identify the ~~cut-off wavelength~~transition wavelength, an example of

which is also shown in Fig. 1. The model-based spectral intensity as a function of the wavenumber k is given by

$$S(k) = \frac{\sigma_w^2 l}{2\pi} \frac{3}{\left(1+\left(\frac{lk}{a}\right)^{2\mu}\right)^{\frac{5}{6\mu}+1}},$$

$$S(k) = \frac{\sigma_w^2 l}{2\pi} \quad 3\left(1+ \quad (3)$$

where μ controls the curvature of the spectrum . Further, a is given as a function of μ:

$$a(\mu) = \frac{\pi\mu\Gamma\left(\frac{5}{6\mu}\right)}{\Gamma\left(\frac{1}{2\mu}\right)\Gamma\left(\frac{1}{3\mu}\right)},$$

where Γ is the gamma function. The and the parameter l is the integral scale of vertical velocity along the horizontal flow trajectory. In this model, l can be expressed as a function of λ_0 and μ (i.e. inverse solution of Eq. (3) in Lothon et al., 2009). The cut-off wavelength can then Further, a is given as a function of μ:

$$a(\mu) = \frac{\pi\mu\Gamma\left(\frac{5}{6\mu}\right)}{\Gamma\left(\frac{1}{2\mu}\right)\Gamma\left(\frac{1}{3\mu}\right)}, \quad (4)$$

where Γ is the gamma function. In our analysis we set $\mu = 1.5$ as it provided a good match with most of the observed spectra. This yields $a \approx 0.69$.

The transition wavelength can be normalized by ~~boundary layer height~~ the depth of the mixed layer z_i to give

~~$$L_0 = \frac{\lambda_0}{z_i}.$$~~

$$L_0 = \frac{\lambda_0}{z_i}. \tag{5}$$

We create the power spectrum from consecutive velocity samples over ~~the same~~ a 30 min interval~~as for σ_w, γ_w, and~~ . The parameter z_i is estimated for each derived spectrum as the local mixed layer depth. For decoupled mixed layers, this is estimated as the difference between the boundary layer top and the estimated decoupling height, taken as the level where vertical velocity skewness changes sign, typically from positive in the lower layers to negative towards the cloud (e.g. Hogan et al. (2009); Ghate et al. (2014)). Here, the boundary layer top is taken as the cloud top ~~altitude determined from a~~ height derived from coincident Doppler cloud radar measurements (the 35.5 GHz MIRA).

~~We~~ In this paper, we also utilise the turbulent dissipation rate, which is derived from the high temporal resolution vertical velocities (O'Connor et al., 2010):

~~$$\epsilon = 2\pi \left(\frac{2}{3a_k}\right)^{\frac{3}{2}} \sigma_{\bar{v}}^3 \left(L^{2/3} - L_1^{2/3}\right)^{-3/2},$$~~

$$\epsilon = 2\pi \left(\frac{2}{3a_k}\right)^{\frac{3}{2}} \sigma_{\bar{v}}^3 \left(L^{2/3} - L_1^{2/3}\right)^{-3/2}, \tag{6}$$

where $a_k = 0.55$ is the Kolmogorov constant for one-dimensional wind spectra, $\sigma_{\bar{v}}$ is the standard deviation of the mean velocity over N sequential velocity samples, L is the spatial length scale corresponding to the number of samples used for calculating $\sigma_{\bar{v}}$, and L_1 is the length scale appropriate for an individual sample. In this study we use $N = 12$ samples, which corresponds

to an averaging interval of 2 min. The length scales are then computed as $L = NUt$, where U is the horizontal wind speed as measured by the Doppler lidar DBS scan sequence, and t is the integration time for one ray. Note that $\sigma_{\bar{v}}$ is calculated over a much shorter time interval than σ_w (2 min vs. ~~30~~60 min).

3 Meteorological conditions and general features

The stratocumulus-topped marine boundary-layer studied here was observed over Mace Head, Ireland, during 24–25 February 2012. ~~The synoptic situation during this period is displayed in Fig. ??.~~ There was a large area of high pressure to the south of Ireland extending west from France out into the Atlantic. To the north were adjacent centres of low pressure west of Iceland and over Scandinavia. The predominant flow over Ireland was from a westerly direction. Our analysis concentrates on the stratocumulus (Sc) clouds emerging after the over-pass of a weak remnant of the tail-end of a precipitating cold front, extending from an occlusion associated with the low pressure centre that had moved from the Northern Atlantic to Eastern Europe by 18:00 UTC on the 24 February~~(Fig. ??).~~ . The passage of the front over Mace Head occurs during the early hours of 24 February, and, by 08:00 UTC, the rain at the surface associated with the front dies out. The remaining mid- and high-level clouds associated with the frontal area have diminished by around 11:00 UTC~~, as shown by vertically-pointing cloud radar observations in Fig. 2~~ . Figure 2 shows the time-height cross-section of the analysed period from a Doppler cloud radar with the stratocumulus clouds emerging after the front has passed. The passage of the front is also evident in the horizontal wind field observed by the Doppler lidar (Fig. ??3) as wind speeds decrease from 15 to ~~8 ms^{-1}~~8 m s^{-1}. This period between approximately 08:00 UTC to 11:00 UTC appears virtually non-turbulent in the observations of the lower atmosphere; the surface front has already passed, but the boundary-layer is still influenced by the presence of the frontal zone at upper levels. The clouds associated with the frontal zone at upper levels are still present. Due to a moderate horizontal flow from the north-west (approximately ~~8 ms^{-1}~~8 m s^{-1}; Fig. ??3), a rather shallow surface based mixed layer with marine characteristics is expected over the observation site. The turbulence characteristics observed

with the lidar are shown in ~~Fig.~~ Figs. 4 and 5, in which the profiles of σ_w and ϵ indeed indicate the existence of a very shallow mixed layer close to the surface. Above ~~150 m~~150 m, the turbulence is very weak with ~~$\sigma_w \leq 0.1\,\mathrm{m s^{-1}}$~~ $\sigma_w \leq 0.1\ \mathrm{m\ s^{-1}}$ and very low ϵ. At these heights, the properties of the flow are more reminiscent of the free tropospheric conditions rather than the boundary layer, although the layer still contains enough particles for a relatively strong lidar signal up to about 1000 m height.

Later during the afternoon of the ~~24~~24th, the north-westerly horizontal flow weakens gradually to about ~~4 m s^{-1}~~ 4 m s^{-1} and remains low until 27:00 UTC (counting from 00:00 UTC of the 24 February), when the wind speed starts to increase. The base of the Sc layer is at approximately the height of ~~1000 m on the 24~~1000 m on the 24th, as observed by both the lidar and radar (Figs. ~~5a and 2~~ 2 and 4). During the 22:00–32:00 UTC period, the cloud base height decreases gradually from 1000 m to about 800 m. The 27:00–32:00 UTC period however features a rather uniform cloud structure with almost constant cloud base height. As shown later, this provides an interesting counterpart for the broken cloud structure seen in the afternoon of the ~~24.~~ 24th.

Cloud topped boundary layers can exhibit many different structural types (Lock et al., 2000; Harvey et al., 2013). The boundary layer mixing is defined as coupled when the cloud layer is directly associated with the turbulent mixing originating from the surface due to buoyant or mechanical turbulence generation, or when turbulent mixing driven by cloud top radiative cooling extends to the below-cloud mixed layer and even all the way down to the surface (Garrat, 1992). The mixing in the boundary layer is defined as decoupled when the ~~cloud driven~~ cloud-driven mixing is not associated with the surface or surface processes. Typically, mixing in and below Sc layers is driven by the longwave radiative cooling of the Sc deck itself, and is important in maintaining the Sc cloud layer through the vertical transport of moisture, especially when there is no substantially strong turbulent vertical transport driven by surface processes.

A broken cloud-deck is evident during the afternoon of the 24 February, caused by breaks between the cellular structure in the stratocumulus advected over the site. The cloud base height shows some variation over time, although mainly less than 150 m, with less variation in cloud top height. We will show later in Sect. 4 that the daytime broken clouds on the ~~24~~ 24th are

associated with decoupled mixing, while the cloud deck in the morning of the ~~25~~ 25th can be regarded as coupled, yet still cloud-driven.

A longer break in the low-level clouds occurs from 18:00–20:00 UTC, which coincides with cirrus clouds emerging over the site. The stratocumulus deck re-emerges when the upper-level cirrus begins to diminish. Unlike the broken field in the cloud deck earlier in the afternoon, which is probably due to internal Sc dynamics, this longer gap appears to be the result of the radiative impact of the cirrus layer above. Christensen et al. (2013) showed that, during night time, on short timescales on the order of a few hours, an upper level cloud significantly decreases the cloud top radiative cooling and the liquid water path of the stratocumulus layer. In essence, part of the up-welling longwave radiation is absorbed and re-emitted downwards by the cirrus and reduces the Sc cloud-top radiative cooling. Without vertical transport of moisture through Sc cloud-top radiative cooling, the Sc layer cannot maintain itself and dissipates. This corresponds very well to our observations, as when the cirrus cloud layer emerging over the Sc deck becomes optically thick, it eventually causes the transitory dissipation of the low-level stratocumulus. Once the cirrus layer is no longer optically thick enough, it does not take long for the Sc layer to return.

4 Turbulence structure in coupled and decoupled cloud driven mixed layers

4.1 Vertical velocity statistics

The time-height cross-sections of ~~turbulence statistics and~~ the lidar attenuated backscatter~~for the full observation period~~ , Doppler vertical velocity and the turbulence dissipation rate are shown in Fig. ~~5 .~~ 4, while Fig. 5 shows the vertical velocity statistics (σ_w and γ_w). The latter also shows the location of the cloud layer, where the cloud base is determined from the Doppler lidar using a threshold of 10^{-4} m^{-1} sr^{-1} for the attenuated backscatter. The location of the cloud-base is not particularly sensitive to thresholds close to this value - e.g. 10^{-5} m^{-1} sr^{-1} gives a very similar result. The cloud top height is diagnosed from the cloud radar, with 50 dBZ used as the threshold for radar reflectivity. Judging by σ_w and the lidar attenuated backscatter

profile, the strongest turbulent variability is generally connected with stratocumulus-topped profiles. It is also evident that σ_w tends to increase towards the cloud deck throughout the observed period. While relatively intense mixing is observed during the 23:00–32:00 UTC period for the whole depth of the boundary layer (with maximum ~~$\sigma_w = 0.8\,\mathrm{ms}^{-1}$~~ $\sigma_w = 0.8\ \mathrm{m\ s}^{-1}$ near the cloud layer and ~~$0.5\,\mathrm{ms}^{-1}$~~ $0.5\ \mathrm{m\ s}^{-1}$ also near the surface), the 11:00–18:00 UTC period shows generally weaker mixing and a more pronounced difference between the near-surface and below-cloud layers. The results imply that the mixing is primarily driven by cloud-top radiative cooling (Lock, 1998; Hogan et al., 2009; Harvey et al., 2013), which is commonly observed in midlatitude marine stratocumulus. The profile of ~~ϵ and γ_w~~ the dissipation rate shown in Fig. ~~5 support~~ 4 supports this conclusion. The collocated Doppler cloud radar observations also indicate considerable turbulent activity within the cloud layer. Other processes that have an impact on the cloud-driven mixing include entrainment, although it is often difficult to separate these processes in remote sensing measurements (Kollias and Albrecht, 2000).

Our interpretation of the boundary-layer structure is further supported when examining the skewness profiles in Fig. 5~~d~~; negative skewness of vertical velocity, which has been shown to indicate cloud-driven mixing (Hogan et al., 2009), is a predominant feature of the below-cloud mixed layer (although it may also occur near the tops of clear-sky surface-driven layers). Moreover, Hogan et al. (2009) noted that cloud-driven mixing in many ways resembles "upside-down" convective mixing, which is supported by the profiles of ~~σ_w and ϵ in Fig.~~ and σ_w in Figures 4 and 5. Similar ~~behaviour~~ behavior has also been observed for in-cloud ~~, i. e. the peak~~ statistics (Frisch et al., 1995; Kollias and Albrecht, 2000) .

Figure 6 shows σ_w, γ_w and ϵ as line plot profiles for consecutive 1-hour segments on 24 Feb (from 11 to 18 UTC), providing more detailed evidence. While σ_w is~~found near the cloud top with~~ , again, seen to peak near or within the cloud layer, the profiles of γ_w and ϵ show the separation between the cloud-driven and surface-based layers on many occasions, with higher ϵ and negative γ_w ~~(Frisch et al., 1995; Kollias and Albrecht, 2000) .~~ being the dominant features in the upper part of the boundary layer. An analysis based on γ_w suggests that the cloud-driven layer is decoupled and that the height of decoupling is found at around 500-600 m at maximum. Unfortunately, we lack collocated thermodynamical profile measurements to

further characterize the vertical boundary layer structure. However, surface measurements of temperature and humidity are used to estimate the lifting condensation level (LCL) (Lawrence, 2005) a shown as the black line in Figure 5. Being clearly below the actual cloud base, this also indicates the existence of a decoupled mixed-layer structure. Moreover, it is noted that operational soundings from Valentia, although about 160 km to the south from Mace Head, share approximately similar meteorological conditions at least during the afternoon of the 24th, and suggest a decoupling height similar to that diagnosed here from the lidar observations after 12 UTC. In some cases, Figure 6 suggests that, for the cloud-driven layer, the depth of influence according to the skewness statistics may penetrate deeper than what would be the actual decoupling height. A case in point is e.g. a sharp increase in ϵ around 500-600 meters for samples after 15 UTC, while the region of negative skewness reaches much lower levels starting from the cloud layer. In contrast to the boundary layer structure seen for the afternoon, Fig. 7 shows a similar plot for 25 Feb (from 0 to 6 UTC) for a deep cloud-driven mixed layer: the profiles of σ_w and ϵ are characteristic of a well mixed boundary layer. Similar conclusion can be made for γ_w as well, noting that its features are quite the opposite (both in sign and the shape of the vertical profile) to what would be expected if the mixing was driven by surface-based buoyancy production. The LCL shown in Fig. 5 (after 24 UTC) is still somewhat lower than the actual cloud base, but they appear to merge towards the morning hours, indicating a gradual reduction in the degree of decoupling.

The evolution of the negative γ_w region ~~indicates~~ suggests a difference in the depth of the cloud-driven layer between the afternoon of the 24 February and the night/early morning of the 25 February~~.~~, which is evident when comparing Figures 6 and 7. A region of weakly positive γ_w extends upwards from the surface during the afternoon of the 24 Feb, suggesting the growth of a surface-based mixed layer, although σ_w is rather weak for this region. The growth of the surface-based layer reduces the depth of the cloud-driven portion of the boundary layer with negative γ_w. No such layer of positive skewness is visible during the ~~25. This indicates that in the afternoon of the 24, the cloud layer becomes decoupled from the surface,~~ 25 Feb. Assuming that the vertical mixed-layer interface can be found by examining the sign of the vertical velocity skewness, the maximum decoupling height is found during 12-15 UTC, while during the night

of the 25 Feb, the cloud-driven mixing is strong enough to support a coupled layer.

~~A very shallow surface-driven mixed-layer is expected over the North Atlantic Ocean because the sea surface temperature is cool, especially in February (10°C). With small surface heat fluxes the ocean surface-driven mixed-layer may only reach a couple of hundred meters or so, with minimal diurnal variation. The presence of a cloud-driven mixed-layer would dominate the boundary-layer throughout the diurnal cycle.~~ The ~~surface-driven layer could therefore be below the minimum range of the instrument and not detected (roughly below 100 m). This is in contrast to land-based surface-driven mixed-layers, which exhibit a strong diurnal cycle and can be much deeper due to much larger surface heat fluxes, even if the surface temperature is not much warmer than that over the ocean. A cloud-driven mixed-layer might be expected to dominate the boundary layer over land during night, but the surface-driven layer could be much stronger during the day. The competition between the two mixed-layers can be observed by examining the turbulent parameters, σ_w, γ_w, and ϵ together~~results in Figures 6 and 7 are very reminiscent of those presented in Ghate et al. (2014) for similar situations. Detecting the decoupling height is discussed further in Section 4.2.

~~A coastal site with an onshore wind should experience a boundary-layer characteristic of marine environments. This shallow surface-driven mixed-layer is then advected over the coastal site.~~ What then causes the surface-based layer to expand during the 12:00–18:00 UTC period? ~~At least two potential~~ Potential factors are identified and explained next. The broken cloud structure seen in the early afternoon could allow increased direct solar surface heating of the coastal observation site, thus promoting growth of the surface mixed-layer. But, due to the close proximity to the ocean and the low angle of the wintertime sun, this effect is most likely weak. The broken cloud structure, and direct solar radiation modifying the temperature profile, could also decrease the production of the turbulent kinetic energy at the top of the cloud layer. However, ϵ remains quite high within the upper portion of the cloud-driven mixed-layer throughout this period. In addition, the surface-based layer starts to extend by noon, before there are any obvious gaps in the cloud layer. The key feature to note is that the horizontal wind speed starts to decrease around noon and continues to do so during the afternoon (Fig. **??**3). With the onshore wind weakening, there is more competition between the shallow

marine surface-driven layer and the deeper surface-driven mixed-layer generated inland; the surface-driven mixed-layer above this coastal location is influenced by both weak heat fluxes from the ocean surface and relatively strong heat fluxes from the land, at least during the day. Further, Fig. 3 suggests some height-dependent fluctuation of the horizontal wind during this period. The fluctuations might act to trigger periods where the stability near the surface is reduced, allowing a surface-based TKE production to affect a deeper layer. In particular, we cannot rule out the possibility of advection of cooler air aloft, which could potentially act as a driver for such events. At the same time, this could also act to slightly increase the stability in the upper portion of the boundary layer, further contributing to the relative strength and extent of the cloud-driven and surface based mixed layers. It should be noted that the surface-based TKE production is primarily quite weak throughout the period, as indicated by the profiles of ϵ in Fig. 6. Moreover, profiles of σ_w suggest that the degree of decoupling is likely moderate, as in most cases there are no particularly sharp changes in the vertical. If considerable surface-based turbulence generation along with the cloud-driven mixing were present, one might expect a minimum of TKE and thus the dissipation rate near the decoupling height. However, this is not clearly seen in our measurements during the afternoon of the 24 Feb, which can be attributed to the general weakness of the surface-driven mixing. Nevertheless, the decoupled structure can be identified, as further illustrated by the scaling of the inertial subrange in the next section. This supports the idea that changes in the stability of the layers would be the reason for changes in the relative depths of influence for the surface-based and cloud-driven layers. It is then understood that a coupled well-mixed layer is formed in this case only with sufficiently intense TKE generation by the cloud-layer, which is shown by σ_w in Fig. 7.

After 18:00 UTC, ~~with no incoming solar radiation, the surface heat fluxes inland are too small to support any surface-driven convection and~~ ϵ ~~at the surface is reduced significantly. There is no competition for the cloud-driven mixed-layer, which can now slowly grow again after~~ is reduced significantly, which appears to be coupled with the dissipation of the cloud driven turbulence and the cloud layer itself. A factor that likely contributes to this is the reduced radiative cooling of the Sc cloud top, due the presence of an overlying cirrus layer between about 17 and 21 UTC (not shown). This period is characterized by positive γ_w near the surface.

However, the significance of this signal is questionable because the width of the vertical velocity distribution becomes very narrow due to weak turbulence at this time. There are also slight changes in wind direction and speed which might cause subtle variations in the vertical velocity moments during this time. As the cirrus layer departs ~~, and eventually reach the surface.~~ after couple of hours and the Sc layer re-appears, the cloud driven mixed layer is quickly re-generated and starts to encroach into the practically non-turbulent surface layer.

4.2 Scaling of the inertial subrange

We now investigate the scaling of the inertial subrange in the stratocumulus-topped periods and relate those results to the differences in the turbulence statistics described in the previous section. ~~As noted earlier, the boundary layer height z_i is defined as encompassing the entire boundary layerfrom the surface to the cloud top altitude, and may contain one or more distinct layers. The cut-off wavelength L_0 is analysed at 30intervals at three normalized height levels in the boundary layer, which are at $0.2\ z_i$, $0.5\ z_i$ and $0.8\ z_i$~~The relative scaling of the inertial subrange L_0 is analysed according to Eq. (5) at two height levels in the boundary layer: one near the cloud base and one in the surface-based regime (yet no lower than a 100 meters to avoid spurious data), based on the estimated decoupling height. We attempt to estimate the decoupling height by finding the level where vertical velocity skewness changes sign, typically from positive to negative when ascending towards the cloud layer, as seen in Fig 5. The scaling of L_0 at the two sampling levels is presented in Fig. ~~8~~8, together with the ~~height of~~ estimated decoupling height at the interface between ~~surface and cloud-driven regimes, diagnosed from the height of zero vertical velocity skewness~~the two regimes. In addition, ~~Fig. 8~~ an alternative version of the surface-based L_0 is provided for comparison ("Surface alt." in Fig 8), where the depth of the cloud driven layer is used instead as the normalizing factor z_i. Figure 8 also shows the below-cloud mean horizontal wind speed, and black shading indicates the presence of cloud (cloud base is retrieved from the lidar, and cloud top from the cloud radar ~~).~~ as in Fig. 5). As the sign of the skewness indicates the direction of the turbulent flux of kinetic energy associated with the mixing, it is expected that the scaling of the inertial subrange would also present differences according to the mixed layer depth and the source of TKE.

It is not always possible to derive L_0; the vertical velocity ~~power-spectra~~ power spectra can be very noisy in regions with low lidar signal strength, or L_0 may be below the wavelengths resolved by the spectral decomposition. Moreover, the spectrum may sometimes feature a double peaked structure, in which case the higher wavenumber peak is considered. The presentation of the results is divided into two equal length periods ranging from 08:00 to 20:00 UTC and from 20:00 to 32:00 UTC counting from 00:00 UTC of the 24 February. In an idealized well-mixed boundary layer with isotropic turbulence one might expect to see $L_0 \approx 1.0$, which is thus highlighted with a solid blue line in Fig. 8. This expectation arises from the first-order hypothesis that the maximum length scale of the turbulent eddies is of the same order of magnitude as the thickness of the ~~boundary~~ mixed layer (Stull, 1988). As shown below, $L_0 < 1.0$ tends to indicate a suppression of the ~~developement~~ development of the turbulent mixed-layer structure. In contrast, $L_0 > 1.0$ can be interpreted as the impact of larger-scale forcings, e.g. gravity-wave activity, or perhaps ~~streching~~ stretching of the turbulent eddy structure during changes in wind conditions. As seen in Fig. 8, overall, L_0 varies significantly with time and with height. Yet, a distinct ~~behaviour~~ behavior is observed with respect to the boundary layer structure and the properties of the overlying cloud-deck.

During 08:00–11:00 UTC, just after the passage of the front and before the stratocumulus emerges over the site, there are clear differences in L_0 with respect to height~~, with $L_0 < 0.5$ at $0.2\ z_i$ and $L_0 \geq 1$ above~~. As the boundary layer is not yet covered by cloud during this time, the samples are drawn from roughly the heights of 100 m and 600 m. The transition wavelength λ_0 is considerably longer for the high-level samples than for those near the surface. This supports the analysis performed in Sect. 3, as it suggests a shallow surface boundary layer with a weakly turbulent, free-tropospheric airmass above, still under synoptic influence of frontal dynamics.

As the stratocumulus layer advects over the area~~around noon, , L_0 is around 1.0 – 1.4 at all levelsfor a brief period before a sharp decrease to $L_0 \approx 0.5$ at 13:00.~~ close to 1.0 in the cloud-driven regime, while in the surface layer L_0 does not present robust scaling. Normalizing the data from the surface layer with the depth of the cloud-driven layer reveals that the transition wavelength near the surface is, nevertheless, generally smaller than at higher levels. At noon, L_0 in the cloud-driven layer peaks to values close to 2.0, associated with a maximum in the

depth of the layer. This coincides with the appearance of a more broken cloud structure, and the growth of the surface-based layer. ~~It is evident from Fig. 8, that, until 20:00~~Between 12 and 15 UTC, L_0 ~~correlates negatively with the height of the zero skewnessinterface. Periods with a pronounced separation between the surface-based and cloud driven layers, (e. g. 13:00–16:00) show characteristically smaller~~ from both sampling levels scales mostly very well with the corresponding mixed layer depths, as diagnosed from the skewness. This provides a good example of the effects of decoupling on both the vertical velocity statistics and the scaling of the turbulent motions. The consistency between the scaling of the inertial subrange and decoupling height derived from skewness is well in line with the interpretation of a decoupled boundary layer outlined in Section 4.1. Afterwards, the skewness-based decoupling height again descends to a very low level: similar to the results from around noon, since the minimum sampling level for the surface-based layer is 100 m, some of the low-level samples for L_0 ~~. Furthermore,~~ may represent the cloud-driven regime. Normalizing λ_0 from both sampling levels with the depth of the cloud-driven layer yields very similar L_0~~values sampled at different levels undergo very similar transitions and have similar magnitudes. The competition between the surface~~ , with slightly suppressed values, i.e. mostly below 1.0. The results suggest that, during periods of pronounced separation between the surface-based and cloud-driven layers~~effectively prevents the formation of a well developed mixed layer, and the clear separation between the two regimes constrains~~ , the skewness-based decoupling height indeed appears to be a useful estimate as it agrees well with the scaling of L_0~~to rather low values. No clear differences can be identified in~~ . In contrast, with less pronounced separation in the profiles of skewness, the actual decoupling height is likely to be found at higher levels than expected, as it would explain the suppression in the cloud-driven L_0~~specific to the mixing regime sampled, but rather, a decoupled Sc-topped boundary layer structure yields similar suppression of~~ ; forcing $L_0 = 1.0$ in the cloud-driven layer after 15 UTC and inverting Eq. (5) for λ_0 yields a decoupling height just below 500 m on average, assuming that cloud top marks the boundary layer top height. This would also produce much better results for the surface-based L_0~~at all sampled levels~~, which have values larger than 2.0 in the case of very low height of the skewness interface. In close agreement, Fig. 6 shows a marked separation in the vertical profile of dissipation rate at the height of 600 m after 15 UTC.

This is actually stronger than what is seen between 12 and 15 UTC, although the opposite is true for skewness.

The situation from 20:00 UTC onwards exhibits somewhat different ~~behaviour~~behavior. From 20:~~00–32~~00 to 32:00 UTC the cloud-deck is almost continuous and there is no solar influence. The cloud-driven mixed-layer grows downwards to reach the surface by 22:00 UTC and remains ~~within~~ in the proximity of the surface until around 32:00 UTC (8 a.m. LT). ~~During the~~ During the first couple of hours (about 20-22 UTC) of the initial growth of ~~this cloud-driven mixed-layer~~ the new cloud driven layer, L_0 ~~values are generally low, although gradually increasing,~~ ~~and~~ scales relatively well with the corresponding layer depths though being slightly smaller than 1.0. Towards and after midnight, L_0 from the higher sampling level gradually approaches 1.0, although it is not until 28:00 UTC that $L_0 \approx 1.0$ ~~at all levels~~(albeit the results show very large temporal variations). Since the minimum sampling height for the surface-based layer was set at 100 meters, it is expected that the normalization by the surface layer depth is not going to work after midnight, since the cloud-driven mixing practically covers the entire boundary layer depth, as shown in Fig. 7. Normalizing the transition wavelength from this height with the cloud driven depth results in L_0 mostly around 0.5, where it stays for the duration of the analysis.

Compared to the daytime period, ~~12:00–16~~between 18:00–24:00 UTC ~~, at night there is no competition for the~~ the mixing close to the surface is extremely weak. Thus, the contribution of the surface-layer to the transport of TKE and the mixed layer structure is low. The re-developing cloud-driven ~~layer as it develops. Rather, the~~ mixed layer can ~~expand~~ encroach downwards quite freely ~~, which is why the suppression of L_0 from~~ during 20:00–26:00 UTC~~is surprising. This~~ , which is clearly seen as the extending region of higher dissipation rate and vertical velocity in Fig. 4 and the negative skewness in Fig. 5. While the suppression of the cloud-driven L_0 at this time may be due to underestimated decoupling height, it may also be influenced by the low horizontal wind speeds, about ~~$4\,\mathrm{m\,s^{-1}}$, which may be affecting~~ $4\ \mathrm{m\ s^{-1}}$, which affects the wind-shear and entrainment processes and thus the dimensions of the cloud-driven turbulence. Before 22 UTC, the surface-layer shows very similar scaling of L_0 as the cloud-driven layer, despite the very weak turbulent mixing. After midnight, the samples near the surface start to represent the cloud-driven layer as well, due to the minimum sampling height of 100 m and

the increasing depth of the cloud-driven layer. Thus λ_0 from both sampling levels is quite similar. The gradual increase in the cloud-driven L_0 during 24:00–32:00 UTC coincides with the increase in horizontal wind speed. The intensifying wind ~~changes~~ may change the aspect ratio of the turbulent eddies by stretching the ~~updraft~~ updrafts and downdrafts further apart horizontally. Additionally, ~~winds~~ changes in wind shear near the cloud top potentially modulate the entrainment process, with intense entrainment causing strong evaporative cooling. This ~~then modifies~~ may modify the production of turbulent energy at the top of the boundary layer (Lock, 1998), which can also affect the scaling of L_0 in the cloud-driven environment. In comparison, it should be noted that λ_0 near the surface does not exhibit a marked increase and corresponds to about half of the boundary layer depth.

Local sunrise is about 7.40 a.m. (31:40 UTC in Fig. 8). A new surface-driven mixed layer starts to grow, evident through positive skewness and a change in dissipation rate in Fig. 5. Although the dissipation rate (Fig. 4c) suggests that this surface-driven layer is less turbulent than the cloud-driven mixed-layer, it continues to grow into, and erode the cloud-driven layer. Note that L_0 at all levels is abruptly reduced to 0.5. Towards the noon of the ~~25~~ 25th the situation is under increasing influence of a gradual airmass change, explaining the reduction in cloud-base height. Related to this, Fig. 2 shows evidence of an enhanced drizzle production, which strongly affects the mixed-layer dynamics, making this situation very different from the earlier analysed periods.

The consequences of the variation in L_0 can be outlined by examining the advective time-scales corresponding to the ~~cut-off~~ transition wavelength of the inertial subrange, λ_0. The time-scales are shown in Fig. 9, and are obtained by dividing λ_0 by the collocated wind speed (averaged over 1 h and 100 m in the vertical). The majority of the timescales reside between 100 and ~~300s~~250 s. As may be expected ~~, time-scales at the lowest height sampled here, $0.2\ z_i$, are usually~~ based on the results above, the time-scales sampled from the surface-based layer are generally somewhat smaller than those ~~above, but this is not always the case, especially in decoupled situations when there are two or more discrete mixed-layers~~from the cloud-driven layer, especially during the peak values found for the latter. These are not only the result of variations in the cloud-driven L_0, but also in the horizontal wind. In contrast, during periods

with clearly decoupled mixed-layer structure, such as that during 12-15 UTC on the 24 Feb, the advective timescales are quite similar for the surface and cloud-driven layers. Knowledge of this time-scale is important when calculating derived products, such as the dissipation rate, from the lidar measurements, where it is assumed that all sampled length scales are within the inertial subrange. More samples would be preferred for more robust statistics, but as indicated in Fig. 9, complex boundary layer structures exhibit a wide variation in the length scales which reside within the inertial subrange~~, especially in the presence of competing mixed layers~~. As an example, when deriving dissipation rate using the method of O'Connor et al. (2010), extending the sampling time beyond 3 min would imply that the spatial length scale L in Eq. (6) is outside the inertial subrange, rendering the assumption used in the derivation of the equation invalid.

5 Conclusions

This study analysed two days (24–25 February 2012) of continuous high-resolution Doppler lidar observations from Mace Head, comprising a long-lived stratocumulus cloud deck following behind an overpass of a cold front.

We focused on the turbulent properties exhibited by the cloud-topped boundary layer through examining various parameters derived from the Doppler lidar vertical velocities. Power spectrum analysis of the vertical velocity was also performed to infer the range of scales of mixing associated with the inertial subrange by defining a ~~cut-off wavelength L_0~~ transition wavelength normalized by the ~~boundary layer depth .~~ local mixed-layer depth (L_0).

From previous studies (Hogan et al., 2009) it is known, that negative skewness of vertical velocity below cloud layer indicates ~~turbulent mixing driven by~~ cloud-driven turbulent mixing e.g. due to cloud-top radiative cooling, which was present throughout the analysed period. During the 24 February, a broken cloud structure was observed in the stratocumulus deck, causing weaker production of turbulent kinetic energy at the top of the boundary layer. Together with decreasing horizontal winds on the afternoon of the 24 February and possible impacts on the stability of the boundary layer, this decreased the depth of the cloud-driven mixed layer, and allowed a weak ~~surface-driven~~ surface-based mixed layer to grow (indicated by positive

vertical velocity skewness). In effect, the cloud deck was decoupled from the surface~~. In contrast, at night on the 24–25, the solid stratocumulus deck was essentially coupled to the surface~~, ~~even though the mixing was~~ although the degree of decoupling was likely moderate, based on the profiles of turbulence statistics. This was supported also by the LCL estimated from surface measurements of temperature and humidity. In contrast, during the night, the degree of decoupling was much lower. The mixing was still cloud-driven ~~, as~~ and the mixed-layer grew to encompass almost the entire depth of the boundary layer. In this case, because the surface-generated TKE was generally low, the extent of the cloud-driven layer depends essentially on the stability conditions and the intensity of TKE generation in the cloud layer, which was strongest during the night.

The investigation of the ~~cut-off wavelength scale~~ normalized transition wavelength L_0 through spectral analysis ~~suggests that a decoupled structure strongly suppresses~~ showed that L_0 ~~at all altitudes. The marked separation between the surface-based and the~~ scales relatively well with the corresponding mixed-layer depth diagnosed from skewness, especially in the cloud-driven layer. The decoupling height between the cloud-driven and the surface layer was estimated as the level where the vertical velocity skewness changes sign from positive to negative, as ascending towards the cloud deck. When a marked separation between the mixed layers was ~~accompanied by a broken cloud structure and rather weak horizontal winds, with~~ present with a relatively high decoupling height as diagnosed from the profiles of skewness, L_0 ~~typically near 0.5 at all heights within the boundary layer . Local intensification of the cloud-driven mixing and the subsequent increase in the depth of the~~ in both the surface-based and cloud-driven ~~mixed-layer seen during the afternoon of the 24 February were accompanied with sharp increases in~~ layers scaled very well with the corresponding layer depths. This agreement between the vertical velocity statistics and the scaling of the inertial subrange corroborates the use of vertical velocity skewness as an indicator of the boundary layer structure. However, in many occasions the surface-based region of positive vertical velocity skewness was less pronounced and the estimated decoupling height was consequently reduced, scaling of L_0 ~~.~~ generally suggested a considerably higher decoupling height than expected based on the profile of skewness.

In comparison, periods with a ~~-~~well-developed coupled (yet cloud-driven) nocturnal mixed layer showed $L_0 \approx 1.0$ ~~throughout the boundary layer, even though before~~ in the cloud-driven layer, following the intensification of the horizontal wind. Before this, L_0 stayed relatively low. This shift is likely the result of shear stress affecting the geometry of the turbulent eddies with increasing wind and also the production of turbulent kinetic energy at cloud top due to changes in entrainment.

~~Prior to the campaign, it was expected that~~ However, near the surface, L_0 ~~would broadly track the fractional depth of the surface- or cloud-driven layerin which the measurement was made. Although this was observed in some situations, typically decoupled layers with competing mixing regimes(13:00–15:00 and 17:00–22:00), it was not a robust indicator on its own. However, the results show that~~ remained suppressed throughout this period.

The results from this campaign show that power spectral analysis of vertical velocity from continuously operated lidars can be used to identify and verify the existence of decoupled mixed layers within the boundary layer. These results are also partially in agreement with earlier studies using profiles of vertical velocity skewness to identify the different mixed layer regimes, although for weakly turbulent surface layers, the vertical velocity statistics were not always robust indicators for the actual decoupling height. Nevertheless, vertically resolved L_0 ~~could provide~~ from continuously operating Doppler lidars provides an additional tool to ~~identify and confirm~~ diagnose the structural features of complex cloud-topped boundary layers and complements the use of statistics profiles in diagnosing the decoupling height. In addition, the identification of potential rapid variations in ~~L_0~~ λ_0 and the reductions seen in decoupled situations are an important consideration when calculating products such as turbulent dissipation rate because of the resulting constraints on the sampling interval for deriving these parameters.

Acknowledgements. This work has been supported by a Väisälä foundation grant from the Finnish Academy of Science and Letters as well as the ERC project PBL-PMES (Grant number 227915). Financial support from the Academy of Finland (project 283030) and the Centre of Excellence Programme (project 1118615) is also acknowledged. The research leading to these results has also received funding from the European Union Seventh Framework Programme (FP7/2007–2013) under grant agreement no 262254. We thank ACTRIS Transnational Access, the Irish EPA ~~,~~and the Irish Higher Education Authority for their support~~, and acknowledge the Met Office Library and Archive for the surface analysis chart~~. Three

reviewers are acknowledged for their constructive comments.

References

Babb, D. M. and Verlinde, J.: Vertical velocity statistics in continental stratocumulus as measured by a 95 GHz radar, Geophys. Res. Lett., 86, 1177–1180, 1999.

Banakh, V. A., Smalikho, I. N., Köpp, F., and Werner, C.: Measurements of Turbulent Energy Dissipation Rate with a CW Doppler Lidar in the Atmospheric Boundary Layer, J. Atmos. Ocean. Tech., 16, 1044–1061, 1999.

Christensen, M. W., Carrió, G. G., Stephens, G. L., and Cotton, W. R.: Radiative impacts of free-tropospheric clouds on the properties of marine stratocumulus, J. Atmos. Sci., 70, 3102–3118, 10.1175/JAS-D-12-0287.1, 2013.

Duynkerke, P. G., Zhang, H., and Jonker, P. J.: Microphysical and turbulent structure of nocturnal stratocumulus as observed during ASTEX, J. Atmos. Sci., 52, 2763–2777, 1995.

Frisch, A. S., Lenschow, D. H., Fairall, C. W., Schubert, W. H., and Gibson, J. S.: Doppler radar measurements of turbulence in marine stratiform cloud during ASTEX, J. Atmos. Sci., 52, 2800–2808, 1995.

Gal-Chen, T., Xu, M., and Eberhard, W. L.: Estimations of atmospheric boundary layer fluxes and other turbulence parameters from Doppler lidar data, J. Geophys. Res., 97, 18409–18423, 1992.

Garrat, J. R.: The Atmospheric Boundary Layer, Cambridge University Press, New York, USA, 316 pp., 1992.

Ghate, V. P., Albrecht, B. A., Miller, M. A., Brewer, A., Fairall, C. W.: Turbulence and radiation in stratocumulus-topped marine boundary layers: A case study from VOCALS-REx. J. Appl. Meteor. Climatol., 53, 117135, doi: http://dx.doi.org/10.1175/JAMC-D-12-0225.1, 2014

Gossard, E. E., Wolfe, D. E., Moran, K. P., Paulus, R. A., Anderson, K. D., and Rogers, L. T.: Measurement of clear-air gradients and turbulence properties with radar wind profilers, J. Atmos. Ocean. Tech., 15, 321–342, 1998.

Harvey, N. J., Hogan, R. J., and Dacre, H. F.: A method to diagnose boundary-layer type using Doppler lidar, Q. J. Roy. Meteor. Soc., 139, 1681–1693, 10.1002/qj.2068, 2013.

Hirsikko, A., O'Connor, E. J., Komppula, M., Korhonen, K., Pfüller, A., Giannakaki, E., Wood, C. R., Bauer-Pfundstein, M., Poikonen, A., Karppinen, T., Lonka, H., Kurri, M., Heinonen, J., Moisseev, D., Asmi, E., Aaltonen, V., Nordbo, A., Rodriguez, E., Lihavainen, H., Laaksonen, A., Lehtinen, K. E. J.,

Laurila, T., Petäjä, T., Kulmala, M., and Viisanen, Y.: Observing wind, aerosol particles, cloud and precipitation: Finland's new ground-based remote-sensing network, Atmos. Meas. Tech., 7, 1351–1375, 10.5194/amt-7-1351-2014, 2014.

Hogan, R. J., Grant, A. L., Illingworth, A. J., Pearson, G. N., and O'Connor, E. J.: Vertical velocity variance and skewness in clear and cloud-topped boundary layers as revealed by Doppler lidar, Q. J. Roy. Meteor. Soc., 135, 635–643, 10.1002/qj.413, 2009.

Jacoby-Koaly, S., Campistron, B., Bernard, S., Benech, B., Ardhuin-Girard, F., Dessens, J., Dupont, E., and Carissimo, B.: Turbulent dissipation rate in the boundary layer via UHF wind profiler Doppler spectral width measurements, Bound.-Lay. Meteorol., 103, 361–389, 2002.

Kollias, P. and Albrecht, B.: The turbulence structure in continental stratocumulus cloud from millimeter-wavelength radar observations, J. Atmos. Sci., 57, 2417–2433, 2000.

Koscielny, A. D., Doviak, R. J., and Zrnić , D. S.: An evaluation of the accuracy of some radar wind profiling techniques, J. Atmos. Ocean. Tech., 1, 309–320, 1984.

Kouznetsov, R., Kramar, V. F., and Kallistratova, M. A.: The vertical structure of turbulent momentum flux in the lower part of the atmospheric boundary layer, Meteorol. Z., 16, 367–373, 2007.

Kristensen, L., Lenschow, D. H., Kirkegaard, P., and Courtney, M.: The spectral velocity tensor for homogeneous boundary layer turbulence, Bound.-Lay. Meteorol., 47, 149–193, 1989.

Lawrence, M. G.: The relationship between relative humidity and the dewpoint temperature in moist air – a simple conversion and applications. Bull. Amer. Meteorol. Soc, 86, 225233, 10.1175/BAMS-86-2-225, 2005.

Lock, A. P.: The parameterization of entrainment in cloudy boundary layers, Q. J. Roy. Meteor. Soc., 124, 2729–2753, 1998.

Lock, A. P., Brown, A. R., Bush, M. R., Martin, G. M., and Smith, R. N. B.: A new boundary layer mixing scheme. Part I: Scheme description and single-column model tests, Mon. Weather Rev., 128, 3187–3199, 2000.

Lothon, M., Lenschow, D. H., and Mayor, S. D.: Coherence and scale of vertical velocity in the convective boundary layer from a Doppler lidar, Bound.-Lay. Meteorol., 121, 521–536, 10.1007/s10546-006-9077-1, 2006.

Lothon, M., Lenschow, D. H., and Mayor, S. D.: Doppler lidar measurements of vertical velocity spectra in the convective planetary boundary layer, Bound.-Lay. Meteorol., 132, 205–226, 10.1007/s10546-009-9398-y, 2009.

Moyer, K. A. and Young, G. S.: Observations of vertical velocity skewness within the marine stratocumulus-topped boundary layer, J. Atmos. Sci., 48, 403–410, 1991.

Nicholls, S.: The dynamics of stratocumulus: aircraft observations and comparisons with a mixed layer model, Q. J. Roy. Meteor. Soc., 110, 783–820, 1984.

Nicholls, S.: The structure of radiatively driven convection in stratocumulus, Q. J. Roy. Meteor. Soc., 115, 487–511, 1989.

Norton, E. G., Vaughan, G., Methven, J., Coe, H., Brooks, B., Gallagher, M., and Longley, I.: Boundary layer structure and decoupling from synoptic scale flow during NAMBLEX, Atmos. Chem. Phys., 6, 433–445, 10.5194/acp-6-433-2006, 2006.

O'Connor, E. J., Illingworth, A. J., and Hogan, R. J.: A technique for autocalibration of cloud lidar, J. Atmos. Ocean. Tech., 21, 777–786, 2004.

O'Connor, E. J., Illingworth, A. J., Brooks, I. M., Westbrook, C. D., Hogan, R. J., Davies, F., and Brooks, B. J.: A method for estimating the turbulent kinetic energy dissipation rate from a vertically pointing Doppler lidar, and independent evaluation from balloon-borne in situ measurements, J. Atmos. Ocean. Tech., 27, 1652–1664, 10.1175/2010JTECHA1455.1, 2010.

Rye, B. J. and Hardesty, R. M.: Discrete spectral peak estimation in incoherent backscatter heterodyne lidar. I: Spectral accumulation and the Cramer-Rao lower bound, IEEE T. Geosci. Remote, 31, 16–27, 1993.

Shupe, M. D., Brooks, I. M., and Canut, G.: Evaluation of turbulent dissipation rate retrievals from Doppler Cloud Radar, Atmos. Meas. Tech., 5, 1375–1385, 10.5194/amt-5-1375-2012, 2012.

Stull, R. B.: An Introduction to Boundary Layer Meteorology, Kluwer Academic Publishers, Dordrecht, the Netherlands, 666 pp., 1988.

Westbrook, C. D., Illingworth, A. J., O'Connor, E. J., and Hogan, R. J.: Doppler lidar measurements of oriented planar ice crystals falling from supercooled and glaciated cloud layers, Q. J. Roy. Meteor. Soc., 136, 260–276, 2010.

~~Met Office surface analysis chart for 18:00on 24 February 2012. (©2012 Crown Copyright, Met Office.)~~

Table 1. Doppler lidar operating parameters for the vertical stare mode during the deployment at Mace Head. System parameters for an individual radial measurement in the DBS mode, where different, are given in parentheses.

Wavelength	$1.5\,\mu\mathrm{m}$
Pulse repetition rate	$15\,\mathrm{kHz}$
Nyquist velocity	$19.6\,\mathrm{m\,s^{-1}}$
Sampling frequency	$50\,\mathrm{MHz}$
Points per range gate	10
Pulses averaged	150 000 (300 000)
Range resolution	$30\,\mathrm{m}$
Integration time	$10\,\mathrm{s}$ ($20\,\mathrm{s}$)
Pulse duration	$0.2\,\mu\mathrm{s}$
Lens diameter	$6\,\mathrm{cm}$
Divergence	$33\,\mu\mathrm{rad}$
Focus	$1\,\mathrm{km}$
Antenna	monostatic optic-fibre coupled

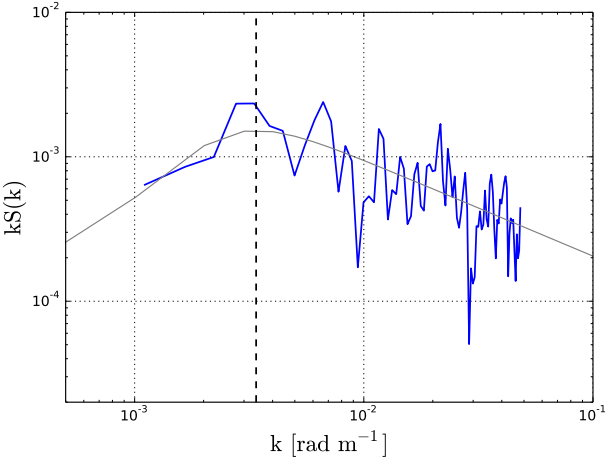

Fig. 1. ~~A schematic figure~~ An example of a vertical velocity power spectral density (S) as a function of the wavenumber k ~~. The red dashed~~ (blue line~~indicates~~) taken from roughly the ~~$-5/3$ slope, fitted on top~~ middle of the ~~spectrum~~ well-mixed layer on ~~the wavelengths that belong to the inertial subrange~~25 February at 4.00 UTC. ~~Also depicted is~~ The thin grey line represents the ~~cut-off wavelength of~~ fit from Eq (3). The black dashed line shows the wavenumber corresponding to λ_0 in this particular example. The inertial subrange ~~(λ_0)~~is found for wavenumbers above this point.

~~Radar backscatter cross section over the two-day period used in the~~

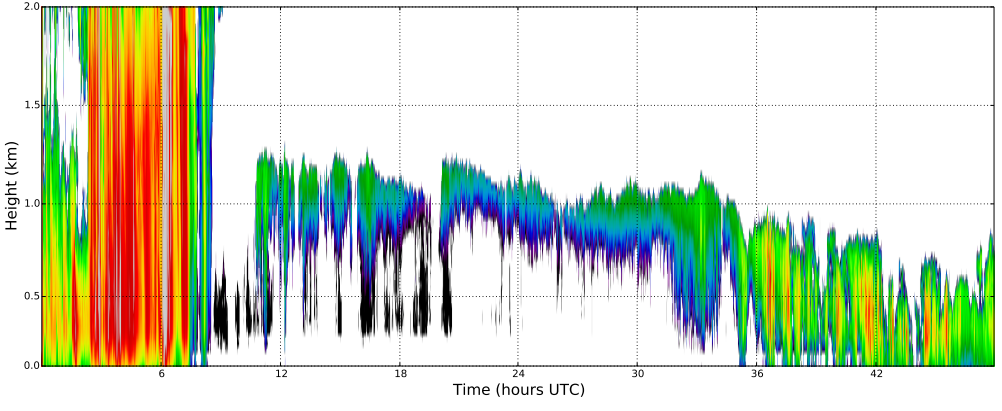

~~analysis.~~

Fig. 2. Radar backscatter cross section over the two-day period used in the analysis.

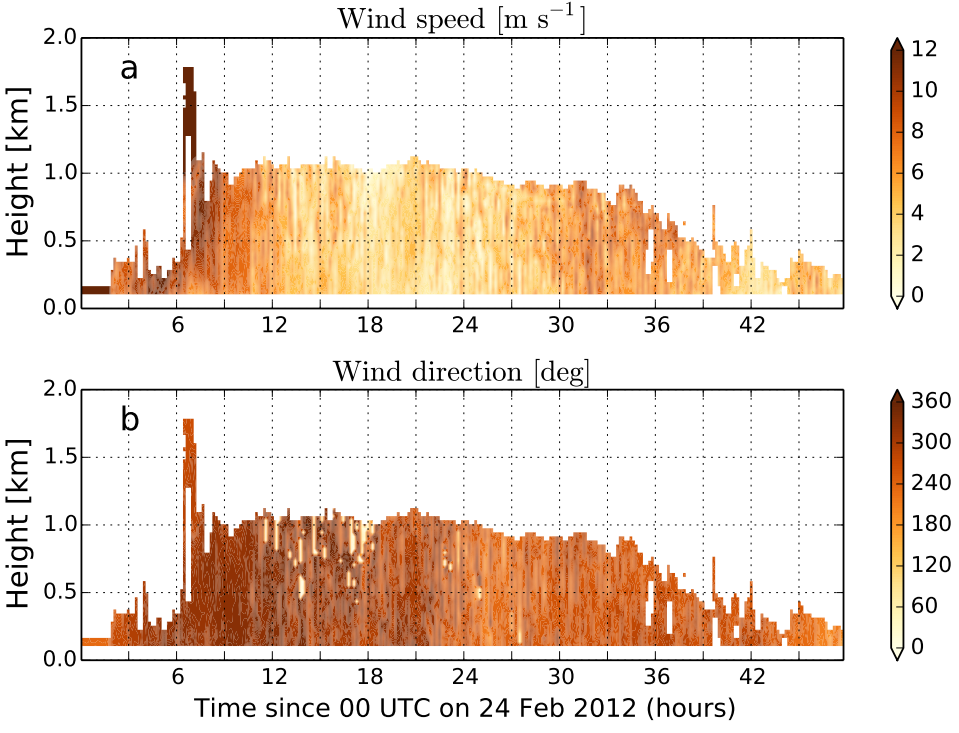

Fig. 3. ~~Profile~~ Profiles of **(a)** the horizontal wind speed and **(b)** direction over the analysed two-day period.~~Wind speed is given by the colormap and wind direction is indicated by the wind barbs.~~

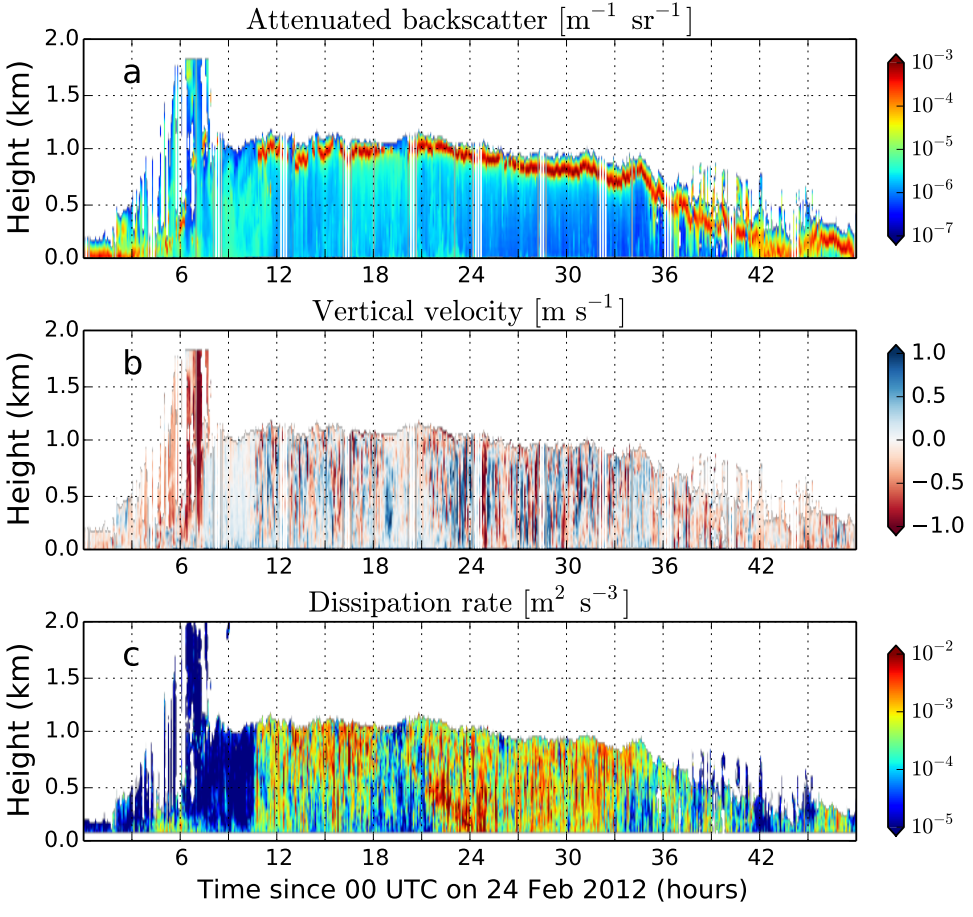

Fig. 4. **(a)** Lidar backscatter, **(b)** Doppler velocity ~~, **(c)** standard deviation and **(d)** skewness of vertical velocity~~ and ~~**(e)**~~ **(c)** turbulence dissipation rate.

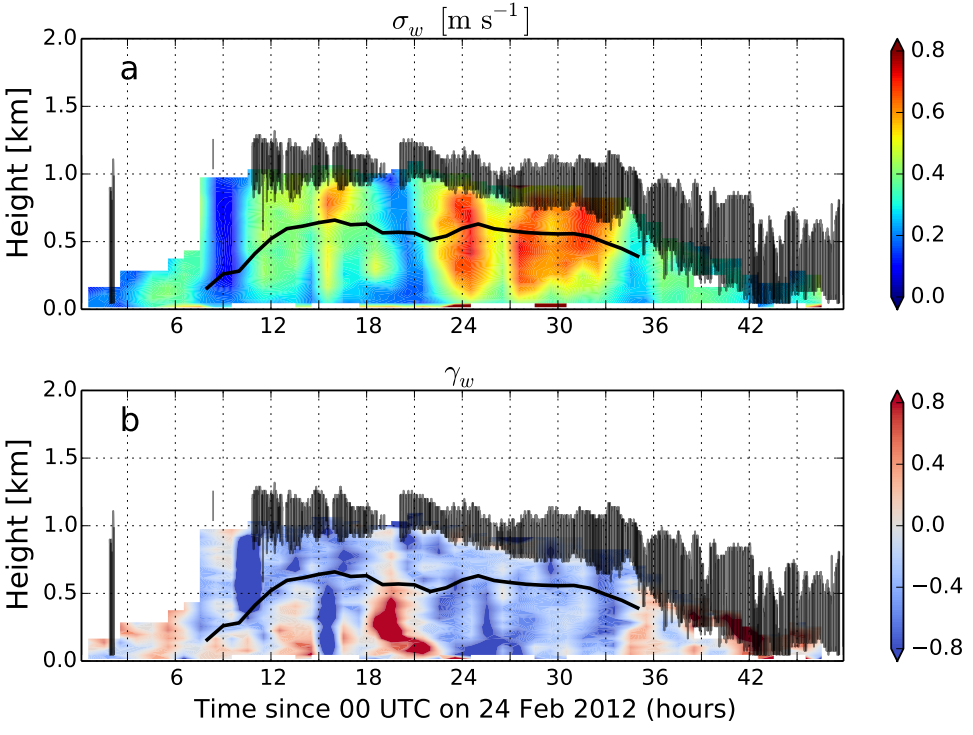

Fig. 5. ~~Scaling~~ **(a)** Standard deviation and **(b)** skewness of ~~the inertial subrange with~~ vertical velocity. The black shading shows the location ~~and extent~~ of the cloud layer~~as~~ , where cloud base is diagnosed ~~using combined sets of~~ from the lidar measurements and radar measurements ~~. Clouds~~ are ~~shown in the upper panel as the black shaded area~~used to infer cloud top height. ~~Blue dashed~~ The black line ~~represents~~ gives the ~~interface between~~ lifting condensation level estimated from surface ~~based~~ temperature and ~~cloud driven mixed layers diagnosed from the profiles of skewness. Red dashed line shows the mean wind speed in the below-cloud layer~~humidity measurements.~~The lower panel shows the normalized cut-off wavelength~~

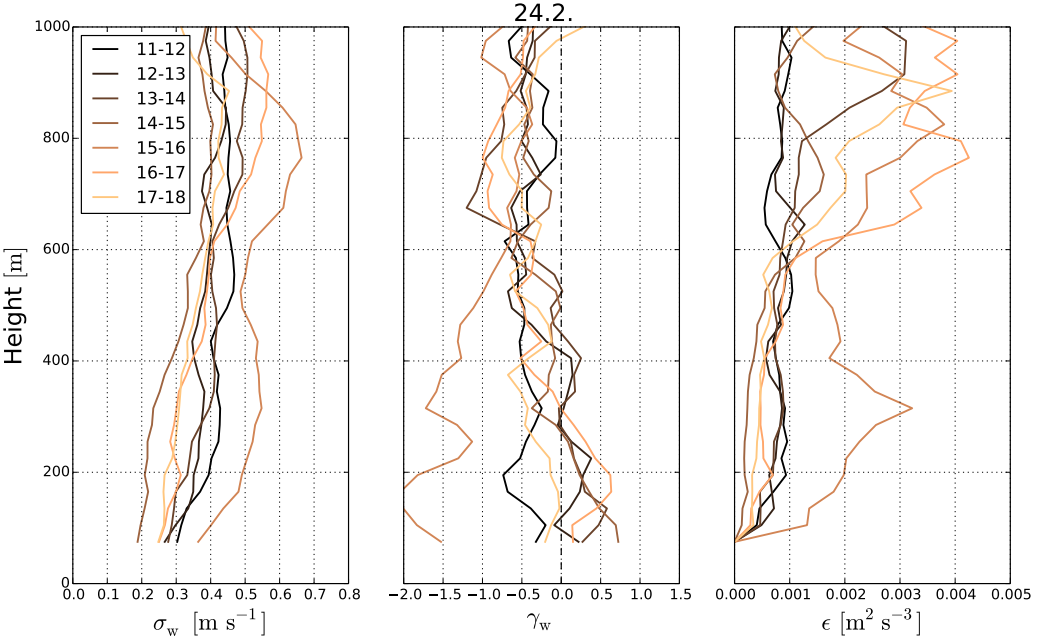

Fig. 6. Profiles of the standard deviation (σ_w) and skewness (γ_w) of vertical velocity, and the dissipation rate (ϵ) for 1-hour segments during the early hours of 24 Feb.

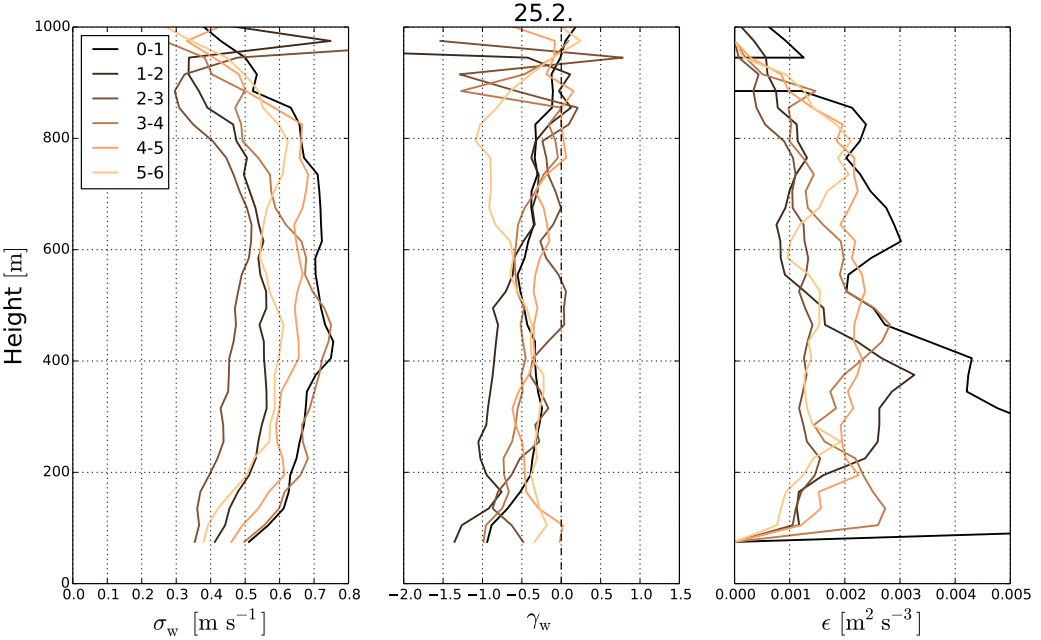

Fig. 7. Profiles of the ~~inertial subrange~~ standard deviation ($~~L_0~~\sigma_w$) ~~with samples from 0.2 z_i shown in black~~and skewness (γ_w) of vertical velocity, ~~0.5 z_i in light blue~~ and ~~0.8 z_i in red markers~~the dissipation rate (ϵ) for 1-hour segments during the early hours of 25 Feb.

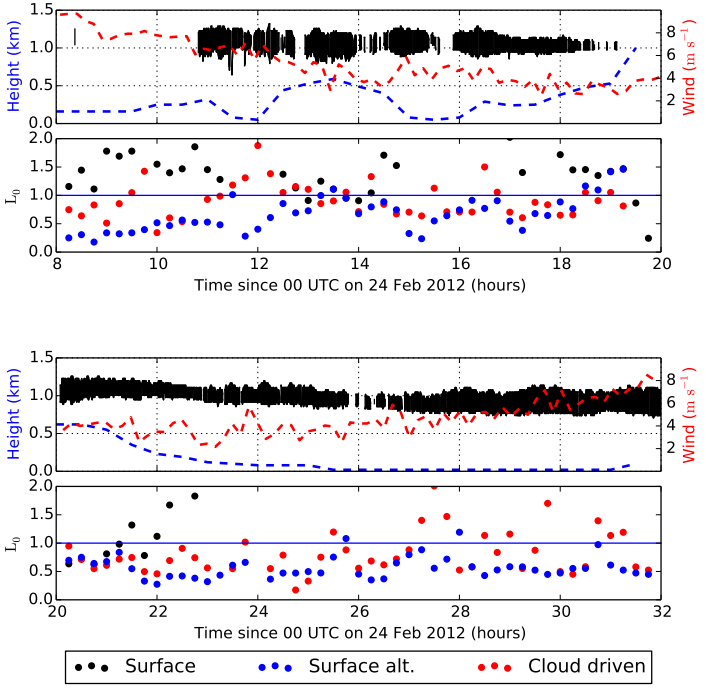

Fig. 8. Scaling of the inertial subrange with the location of the cloud-layer shown in the upper panel as the black shaded area. For this, cloud base is diagnosed from the lidar measurements, while radar measurements are used to infer cloud top height. Blue dashed line represents an estimate of the interface between surface based and cloud driven mixed layers, approximated as the level where vertical velocity skewness changes sign from positive to negative. Red dashed line shows the mean wind speed in the below-cloud layer. The lower panel shows the normalized transition wavelength of the inertial subrange (L_0), which is sampled from the 1) cloud-driven and 2) surface-based layers, yet no lower than a 100 meters to avoid spurious data. Two versions of the surface-layer samples are shown: "Surface" shows L_0 normalized by the surface-layer depth, while "Surface alt." shows the same data but normalized with the cloud-driven layer depth.

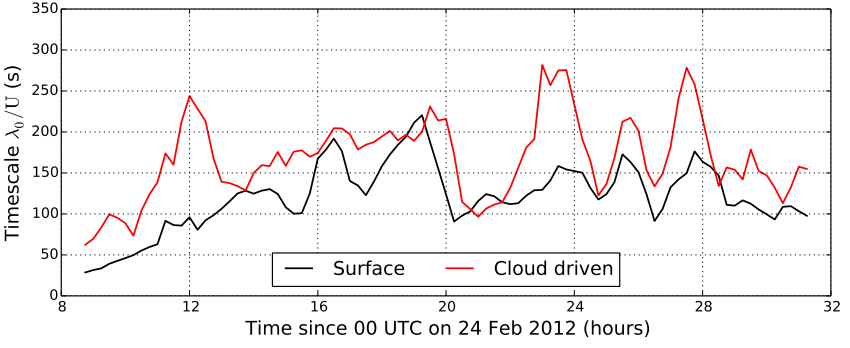

Fig. 9. Advective time-scales corresponding to the largest scales within the inertial subrange (λ_0) shown in Fig. 8 from ~~three heights. Time-scales from 0.2 z_i are shown in back, 0.5 z_i in light blue~~ the surface-based (black) and ~~0.8 z_i in~~ cloud-driven layers (red). U denotes the horizontal wind speed.